Bachelor Thesis

Stockholm University

Degree Project in Geology 30 hp

Geophysical research of the Granby structure - support for an impact origin

Rickard Exner

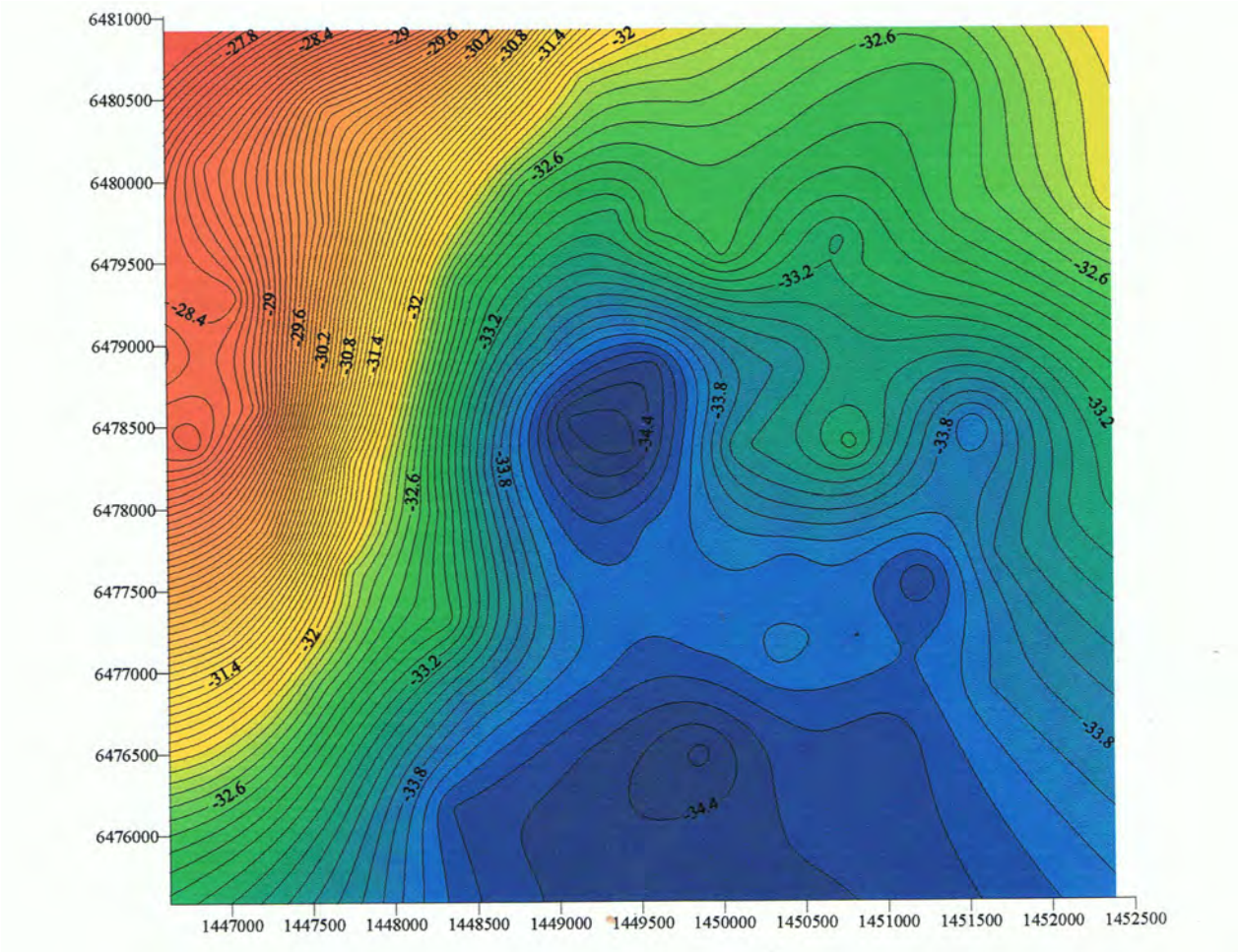

Stockholm 2013

Department of Geological Sciences
Stockholm University
SE-106 91 Stockholm

Abstract

This work is a geophysical study of the Granby structure in the vicinity of the town Vadstena in south-eastern Sweden. The structure has been described as a probable meteorite crater penetrating Paleozoic sedimentary rocks and the crystalline Precambrian basement, with a depth of 270 m below surrounding crystalline basement and a rim that rises in some places 70 m above surrounding basement. With a soil coverage of 20 – 40 m the crater have a maximum depth of 377 m below surface. The shape is described as oval with a width of 2 km in the N-S direction and up to 3 km in the W-E direction (Wikman et al. 1982). The goal of this investigation is to describe the shape of the structure and the extent of the brecciation into the surrounding crystalline bedrock. The means to reach this goal have been geophysical measuring techniques. Measuring the gravitational anomaly in a net covering the crater and its surrounding area has resulted in a gravity map that is more detailed than earlier studies. Further, modeling has been used to give a generalized picture of the shape of the crater and the extent of its influence on depth of the crystalline bedrock surrounding it. Ground magnetic measurements covering the rim, together with the pre-existing air magnetic map, have given a more detailed picture of the spatial extent of the crater and indications of the placement and form of the rim.

1 Introduction

1.1 History of impact studies

The following section is a summary of *Themes in the study of impact cratering* (Melosh 1989). Studies of impact craters began with Galileos observations of craters on the Moon 1609 and the publishing of his Sidereus Nuncius (The Starry Messenger) 1610. Despite this, several centuries passed before the processes were understood and all those in doubt were convinced. Not until the 20th century impact cratering has been recognized as a separate branch of science. One crucial factor that made the impact theory for the craters on the Moon hard to believe was the fact that almost all of the craters were circular. Experiments had shown that oblique impacts would create elliptical craters and it was not likely that so few of the impacts would have been oblique. However, in the beginning of the 20th century the comparison between high velocity impacts and explosions was made and the conclusion was reached that circular craters were created for impacts at almost all angles. This was an important step to understand how impact craters are formed. 1906 the first accepted connection between craters on Earth and impacts was made when D. M. Barringer showed that the now called Meteor Crater in Arizona, USA, is of meteoritic origin. In the 1920s and 30s more and more craters with meteoritic origin were found on Earth. A term that mislead the conceptions for a while was crypto-explosive structures, which was used for many of the formations that later would be recognized as impact craters. Understanding of shatter cones and the findings of the high pressure facies of quartz, coesite and stishovite, gave a deeper understanding of the processes that takes place when a body impacts with high velocity. E. M. Shoemaker began in the 1950s to investigate Meteor Crater and compare it to a crater formed by a nuclear tests, the Teapot Ess.

He discovered the inverted stratigraphy on the rim of the crater and formulated a theory about the formation of impact craters, which was published in 1960 and 1963. The theory is thought to be of vital importance for the science of impact cratering.

1.2 Crater morphology

Craters are normally divided into simple craters, complex craters and multi-ring basins (Melosh, 1989).
The *simple crater* is bowl shaped with a circular raised rim. If they are created by bodies moving slower than a few km per second they are often more irregular and have a broad poorly defined rim. Such craters are created by material thrown out of the initial impact crater. The upper limit for simple craters is restricted by gravity as the formation at a certain size collapses. According to Melosh and Ivanov (1999) this occurs at a diameter of about 15 km diameter on the Moon. But on Earth,, which has a gravity six times greater than the Moon, it occurs between 3 and 5 km. Most terrestrial simple craters are smaller than 4 km and the transition range seems to depend on whether the crater is formed in crystalline or sedimentary rocks. A lens of broken rock debris and shock-melted rock normally fills the crater up to half of the rim to floor depth and the depth from the rim to the bottom of the breccia lens is about one-third to one-fifth of the crater diameter. Investigations of breccias filling simple craters have shown that the craters forms by a straight-forward collapse of the rim immediately after the impact.

In larger impacts the crater collapses after its creation and landslides and faults create a steep, sometimes broken rim with a relatively flat floor inside. This is what is called a *complex crater*. Because of this collapse, the diameter of the complex crater is much greater compared to its depth. A central rise occurs through isostatic uplift. According to Grieve (1987), among others, the occurrence of an uplifted central core is the principal difference between the two types of craters. The central uplift evolves at smaller sizes in sedimentary rocks compared crystalline. Among Fennoscandian craters the lower limit for central uplift in basement rocks seems to be about 8 km (Henkel 1992) while in sedimentary rocks it is about 4 km according to Grieve (1988). In even bigger impacts the central rise may be replaced by a rised ring with irregular peaks and is then called *ring peak crater*.

When extremely big impacts occur it seems to influence the very tectonic building of the planet and several rings, for example five in the enormous Orientale crater on the Moon (Melosh and Ivanov 1999), may be created. These are called *multi-ring basins*.

1.3 Cratering mechanics

The following section is mainly based on information in Melosh (1989). The minimum encounter velocity for a projectile, hitting Earth, is 11.2 kms^{-1} (asteroids) and the maximum 72.8 kms^{-1} (comets). The first thing a meteorite falling towards Earth will meet is the atmosphere. This encounter with gases at high speed will vaporise a part, or all, of the meteorite. The minimum diameter of meteorite needed to penetrate the Earth’s atmosphere, retaining sufficient velocity to create a high-velocity impact, is computed by Melosh (1989) and given for vertical incidence for ice, stone and iron. An ice-body need a diameter of 150 m,

a body composed of rock material 60 m and an iron-body 20 m. Smaller bodies may penetrate the atmosphere and hit the surface but the processes of those hits are different than the high-velocity impacts. Such bodies can be found intact. Even smaller bodies, so called “cosmic dust” may even be slowed down gradually and eventually come to rest in the upper atmosphere. Larger bodies continue down and reach the lower denser atmosphere where the compressed atmospheric gases in front of the meteorite are heated up. The gases radiate their heat to the body, which begins to melt and vaporize. The hot atmospheric gases, meteoritic vapor and melt droplets may emit a bright light visible on Earth. The shock waves produced in front of the meteorite may be devastating and is the first force that hits the ground. As the meteorite passes through the atmosphere the extreme pressure often breaks it up and it hits the surface in a cluster of fragments, creating a crater field or strewn field. Only very tough stone or iron meteorites can penetrate the atmosphere without being crushed. When the meteorite reach a certain size, from about 10^5 to 10^{10} kg on Earth, the fragments will produce craters that overlap and fill the whole scatter area, thus producing the appearance of one single crater. The craters produced by clusters are generally shallower than the craters created by solid meteorites.

The first stage of impact cratering begins with the projectile *contacting* the surface. The projectile pushes target material out of its path, compresses it and accelerates it to almost the velocity of the projectile. The shock wave created between the target and the projectile spreads and propagates into both target and projectile and they may both melt and vaporize. Strongly shocked and melted material squirts out in “jets”. When the projectile has unloaded all its energy to the target, the first stage, contact and compression, is over and it doesn’t take more than a thousand to a tenth of a second. The shock wave propagates into the bedrock in a close to hemispherical form with almost constant thickness. The pressures are largest directly below the impact but do not vary much over the hemisphere. It has a rate of decline that ranges between $1/r^{1.5}$ for small impacts to $1/r^3$ for the highest velocity impacts. In the shock both pressure and particle velocity is high but behind the shock the pressure drops to nearly zero while the particle velocity declines to a residual level of one-third to one-fifth. This remaining acceleration is what eventually leads to the excavation stage, which is further described below. The hemispheric shock wave is centered some distance below the surface and therefore hits the surface from below (Fig 1.1). Since the surface is a plane of zero pressure a physical dilemma is created as the shock wave meets the surface. To solve this, a rarefaction wave of equal strength but opposite sign is created as soon as the shock wave arrives, propagating downward. The sum of the two waves is always zero. Points near the surface are hit by the rarefaction wave almost at the same time or shortly after the shock wave, which then is reduced so that maximum pressure is never reached. Deeper points are hit by the shock wave and reach maximum pressure before the rarefaction wave arrives. The sudden change from very high to very low pressure as the rarefaction wave replaces the shock wave creates a tension. The tension is higher in the deeper parts where the maximum pressure is reached before it is replaced by the very low pressure of the rarefaction wave. The tensional stress leads to cracks in the target rock that lengthen at very high speed and link up. The target rock loses cohesion and the material turns into a mass of broken fragments, a breccia. The brecciation is thought to reduce by the square of the distance from the impact centre. As the shock wave expands further it weakens and degrades first into a plastic stress preceded by an elastic precursor and then into an entirely plastic wave that continues throughout the planet.

Immediately following this first stage, the second stage begins – the *excavation* stage. The shock wave initiates a movement of the target material, which begins to move outwards in directions approximately radial from the point of impact. As said earlier the velocity of the material is between one-third and one-fifth of the peak particle velocity in the shock,, which is about one-half of the impact velocity. Because of the rarefaction wave propagating downwards from the target's free surface an upward-directed pressure gradient is produced. This tends to deflect the particles trajectories towards the surface, which results in curved streamlines (Fig. 1.2). This leads to an excavation that opens a crater many times larger in diameter than the projectile that hit the target. This flow is much slower than the shock wave and by the time it is fully developed and the crater begins to grow the shock wave has long before passed. Some of the material close to the surface looses contact with their neighbors and ejects outwards from the growing crater in ballistic trajectories. This ejecta curtain forms the outer edge of the growing crater and results in an allogenic[1)] breccia layer surrounding the crater. The streamlines of the excavation flow cut across the contours of maximum pressure and the ejected material thus contains contributions from all the different shock levels. The deeper materials that move to the sides and upwards and don't loose contact, forms the raised crater rim. Studies have shown that approximately half of the height of the rim is due to this uplift and a large portion of the rest is built up by ejected debris deposited on top of the uplifted surface. There is however other contributions such as breccia lenses injected into the crater wall. The ejected material is thrown out at a low velocity and often retains its stratigraphy, however overturned. This stage may last for seconds up to minutes depending on the size of the crater.

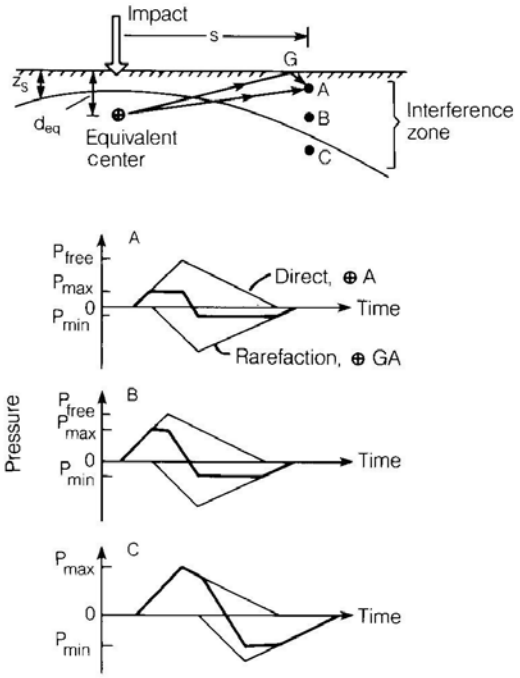

Fig. 1.1. The stress wave radiates from the equivalent center at depth d_{eq} below the target surface. At point A the direct wave arrives shortly before the rarefaction wave and the net pressure is strongly limited. At point B the rarefaction wave arrives later and allows the pressure to rise higher. At point C the rarefaction wave arrives after the direct wave has reached its peak and no pressure reduction occurs. (From Melosh 1989)

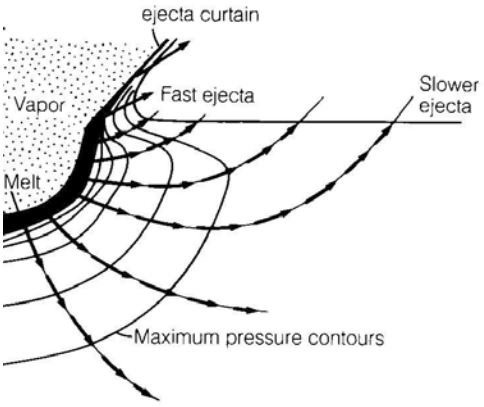

Fig. 1.2. The arrows illustrate the excavation flow with the deflected particle trajectories. Also shown is the ejecta curtain. (From Melosh 1989)

The last stage is *modification,*, which begins after the crater has been fully excavated. During this stage debris slides down the interior walls, filling the crater with a breccia often combined

with impact melt and parts of the rim. This collapse is mainly due to gravity but elasticity of underlying rock may also be of importance and it creates a crater with inner rim walls dipping close to 30° (the angle of repose). The slopes gradually lessen towards the center, which may form a flat floor. This applies to simple craters, which on Earth mean craters with a diameter of up to approximately 4 km. In larger craters, complex craters, slump terraces may form on the rim walls and one or several central peaks or even rings of mountains may form inside the crater often surrounded by a flat floor. This modification of the crater shape is apparently achieved by collapse driven by gravity. The collapse starts with a stratigraphic uplift of the

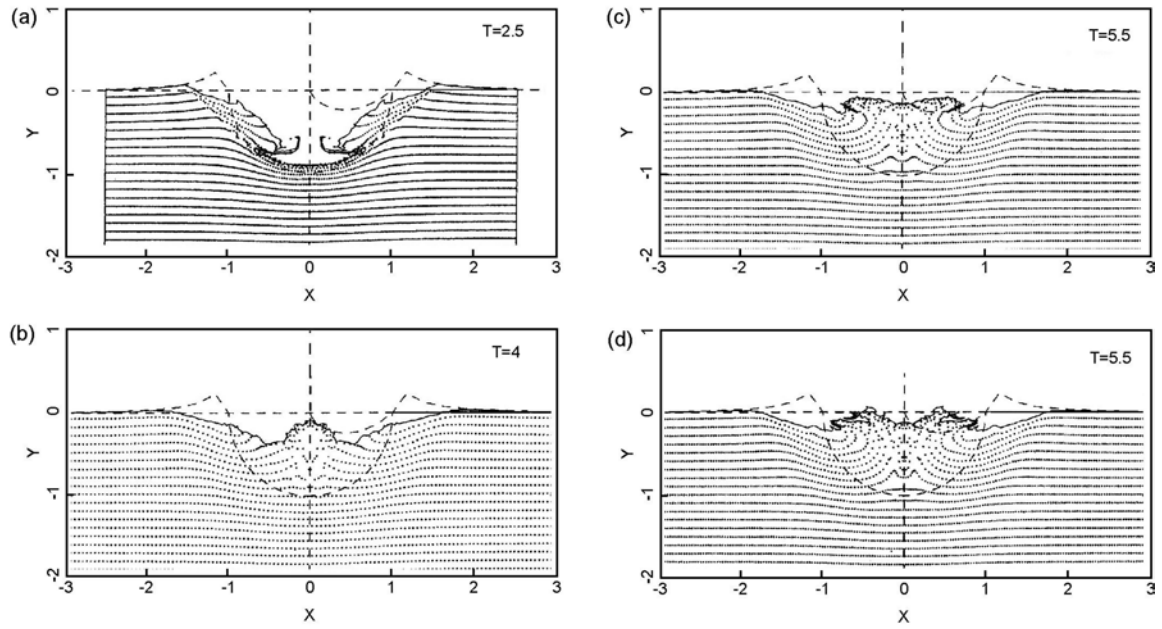

Fig. 1.3. The final shape of collapsed craters with diameter of ~2 km (a), ~20 km (b), ~40 km (c) and ~80 km (d). Dashed lines show the initial contour of the transient crater and (right) the ejected volume. The initially flat layers (dotted lines) are distorted. The length unit is equal to the maximum transient cavity depth. Somewhere between 20 km (a) and 40 km (b) the uplift collapses and instead of a single peak forms a ring of mountains surrounding a cavity. (From Melosh and Ivanov 1999)

rocks underlying the crater's centre followed by rock units near the rim slumping inward and downward. In larger craters, with sizes from approximately 30 km (Fig. 1.3) the uplift begins to experience an overshoot above the original target and falls down before it comes to rest. This produces a pit at the top of the uplift and a peak ring structure develops surrounding the uplifts former site. Several theories have been presented and developed to explain the mechanics of this collapse. The most recent is the theory of acoustic fluidization developed by Melosh and Ivanov (1999). It suggests that strong vibrations transmitted as a sound wave via rock-to-rock contact can make rock debris flow like a fluid, even in the absence of water or air. Other theories suggest that the rock debris is fluidized by impact melt or by the presence of some interstitial fluid like water or fine-grained breccia. The central uplift and rings have been compared to the same created when a drop of water hits a surface of water. Melosh (1989) even suggests that when the acoustic energy is large, the debris in the crater may slosh back and forth in the crater. However, when the energy is lowered the rock debris material becomes rigid again and comes to rest as peaks or rings of peaks.

2 Geophysical data

2.1 Gravity and density

The differences in density, porosity and frequency of fractures of different rocks create differences in the gravity field that can be measured with instruments called gravimeters. (Parasnis 1979; Milsom 1996)

The SI-unit for gravitation is m s^{-2} but as it is too large for geophysical studies the unit gu (gravity unit) or µm s^{-2} is used instead. Earlier, and in many cases still, the unit gal (cm s^{-2}) (after Galileo) and its sub-unit mgal (1 mgal = 10 gu) is used.

The gravitational field of Earth is almost that of a sphere but has a slight increase towards the poles due to the elliptic form of the Earth. The difference between the poles and the equator is approximately 0,5% or 50 000 gu. The international gravity formula, adopted in 1967 by the International Union of Geodesy and Geophysics, gives the variation of the gravitation with the latitude λ, at sea level.

$$g_{norm} = 9\ 780\ 318.5 + 51\ 629.27 \sin^2\lambda + 229.5 \sin^4\lambda \quad \text{(gu)} \tag{2.1}$$

Although both an older (1930) and a later (1980) version is available, the 1967 version is still most frequently used since a change of formula would mean that all already accepted values for base stations all over the world would have to be changed as well.

The gravitation at sea level according to formula 2.1 is at the equator 9 780 318.5 gu and at the poles 9 832 177 gu. In geophysical studies the measured anomalies range between a couple of thousands down to a few tens of a gu, thus a significantly smaller value than the overall gravity.

The SI-unit for density is kg m^{-3} but often Mg m^{-3} is used. Most rock types in the crust have densities between 2.0 and 3.2 Mg m^{-3}. A standard density for the upper crust often used in crystalline areas is 2.67 Mg m^{-3}.

2.1.1 Gravimeters

Three main types of gravimeters are used today, stable, unstable and dynamic. Dynamic is not usually used in geophysical studies and is therefore not further considered here.

The stable systems are roughly based on a mass attached to a spring that is drawn from its equilibrium by gravity. The extremely small motion is then amplified optically, mechanically or electrically and read on a scale.

The unstable systems, also called astatic, have more than one spring. A schematic of the principal is shown in Fig. 2.1. The weight *m* is pivoted at *P* and is supported against gravity by the spring *A*. An increase in gravity will cause the arm to rotate around *P*, which will not

only increase the length of spring *A* but also decrease the angle θ. A beam (created by a light source *F*) is deflected by the motion and reflected on a scale *S*. The pull on a second spring *B*, necessary to return *m* to its normal position, is measured as well as the time it takes for the beam to return to a fixed point on the scale. Since the second spring *B* does not have to support the mass *m* against gravity it can be very weak and hence very sensitive to small changes in gravity.

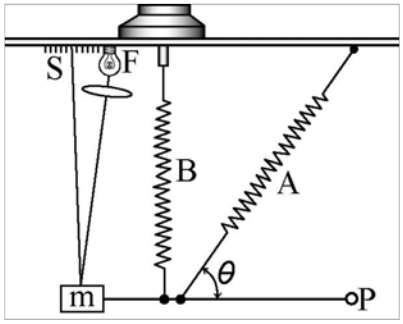

Fig. 2.1. Schematic of the operating principle of an astatized gravimeter. (From Howell 1959)

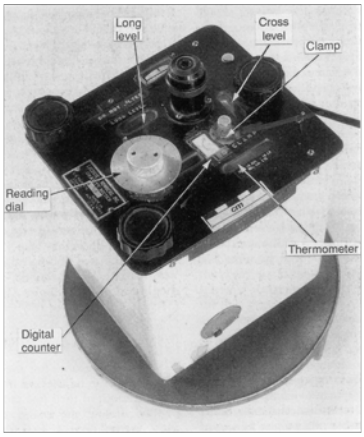

Fig. 2.2. A LaCoste-Romberg gravimeter.

In this study a LaCoste-Romberg astatic gravimeter was used (Fig. 2.2). This instrument is different from other gravimeters in the sense that it has one single long adjustment screw (to adjust the pull on the mass by the second spring), which means that it may be used at any position on Earth without having to be reset. The LaCoste-Romberg gravimeter requires a stable temperature, which is upheld by the power of a battery. When the instrument has attained the proper temperature and upheld this for two to three hours it has a very low drift, which is even possible to extrapolate over short periods of cooling. The low drift makes readings at a base station necessary not more than a couple of times a day, provided that a tidal correction (see below) is applied. The instrument is calibrated in mgal.

2.1.2 Gravity reductions

Corrections are made to reduce large and calculable effects produced by sources not of geological interest for the study. If these effects are positive, e.g. have a component in the direction of the Earth's main field, the reductions are negative and vice versa. The reductions made are for latitude, elevation above sea level (free air reduction), density above the reference datum (Bouguer), terrain variation, tidal effects and drift correction (Milsom, 1996).

Latitude correction

Normally the Earth's main gravity (calculated with formula 2.1) is subtracted from the observed gravity. Alternatively the theoretical north-south gradient ($8.12 \sin 2\lambda$ gu km^{-1}, where λ is the latitude difference in degrees from a local base station) is used. The number is subtracted southwards from the base station and added northwards.

Free air correction

This correction is dependent on the height above the sea-level reference surface. An increase in height means a greater distance to the Earth's centre of mass and therefore a lower gravitation is observed. Consequently a negative effect and a positive correction are applied.

If measuring takes place under the sea-level reference surface the effect is positive and the correction negative. The free air correction is normally said to be equal to 3.086 gu m^{-1}.

When these two corrections are made a so called free air anomaly or free air gravity is obtained.

Bouguer correction

The Bouguer correction reduces the effect of the masses between height of the gravity station and the sea-level reference surface. For simplicity the generalization is made that the mass is equal to a plate of equal thickness and mass extending to infinity in all directions, a so called Bouguer plate. The effect is positive and equal to $2\pi\rho Gh$, where h is the plate thickness, ρ is the density and G is the gravitational constant ($6.67*10^{-11}$ N kg^{-1}). The correction,, which is negative, is 1.1119 gu m^{-1} for the standard density 2.67 Mg m^{-3}.

When this correction is made on the free air gravity, a so called Bouguer gravity is obtained.

Terrain corrections

If the terrain is highly undulating more detailed topographic corrections have to be made. The corrections can be made directly, without making the Bouguer correction, but it is easier to do them on the calculated Bouguer gravity in, which case the corrections are always positive. Terrain corrections are made by computer using digital elevation data (in Sweden with 50 m spatial resolution).

When terrain corrections are made a terrain corrected Bouguer gravity is obtained.

Tidal correction

The relative positions between the Earth, Sun and Moon affects the gravity in 12 and 24-hour cycles and may exceed 2.5 gu. These variations are difficult to calculate without computers. When repeated measurements at the base station are made in ca 3 h intervals, this effect can be removed together with the instrument drift correction.

Drift corrections

The instrument drift is due to creep like the change of the properties of the springs with time. To be able to correct for the drift, readings at the same place (a base station) several times a day have to be made. The drift is assumed to be linear between these readings. The corrections are subtracted or added to the readings dependently so that the difference at the base station always equals zero. If the readings on the base station are made twice a day (first and last readings of the day) the tidal correction should be made separately. If the base station is measured more often, for example every third hour, the tidal and the drift corrections are made simultaneously.

2.2 Magnetism and susceptibility

The magnetic fields of geological bodies are superimposed on the Earth's main field (Milsom, 1996). It may be measured by instruments called magnetometers.

The magnetic field strength is now usually measured in the unit nT (nanoTesla), which is numerically equal to the older unit gamma.

The Earth's magnetic field is approximately dipolar with an inclination of about 11º to Earth's spin axis. Due to the inclination, the magnetic and the geographical pole differ. The magnetic field also changes slowly with time in magnitude and direction. The variation of the Earth's field with latitude, longitude and time is described by the International Geomagnetic Reference Field (IGRF). In the investigated area the inclination (the angle between the magnetic field and the Earth's surface) 73º is used and the total intensity is approximately 50 000 nT.

When a body is placed in a magnetic field it acquires a magnetization. The ability to be magnetized is called magnetic susceptibility and is small for most materials. It may be negative (diamagnetism) or positive (paramagnetism). These small magnetic fields scarcely affect magnetometers. A few materials, of, which magnetite is the most important, are more magnetic (ferromagnetic or ferrimagnetic) and may create a magnetic field strong enough to be seen as an anomaly in magnetometer surveys.

When the rock is brecciated it allows water and air to come in contact with the magnetic components and oxidize them, magnetite to hematite,, which reduces the susceptibility (Henkel & Guzmàn, 1992).

2.2.1 Magnetometers

Until about 1960 so called torsion magnetometers,, which used compass needles mounted on horizontal axes, were used. They were then replaced by ground versions of the fluxgate and proton precession magnetometers used for airborne surveys. The fluxgate magnetometers use one or more cores of magnetic alloy with coils through, which a current is passed. Variations in electrical properties with magnetization are converted into voltages proportional to the external field. The proton precession magnetometer consists of a bottle with low freezing point hydrocarbon fluid with a coil of copper wire. As a current is passed through the coil a strong magnetic field is produced. The hydrogen nucleus (protons) of the fluid aligns their spin along this magnetic field until the current is switched off and they realign in the direction of the external field. They precess about the magnetic field direction at a frequency proportional to the field strength. This frequency is measured by phase-sensitive circuitry down to an accuracy of 1–0.1 nT. The drawbacks are that they may give erratic readings where there are strong field gradients and they may also be interfered by power lines, radio-transmitters and other things that produce a magnetic field. However, the readings are given as drift-free absolute values in nT, which only have to be corrected for diurnal variations.

2.2.2 Magnetic corrections

To correlate for the diurnal variations a second instrument can be used by making readings at a base station at three to five minutes interval. This way a complete diurnal curve can be constructed. If only one instrument is available, as the case was in this survey, repeated visits to a base station at intervals of less than one hour have to be made. The main sources of erratic readings are magnetic interference from power lines, traffic, buildings etc. and battery failure.

3 Granby – location and geology

The Granby structure is located close to the small community Granby in the vicinity of the town of Vadstena, Östergötland, Sweden (map area 8E NO HJO) (Fig. 3.1). The centre of the crater is located in the bog Fyllamossen, at coordinates 1449000 E 6478500 N (Swedish grid).

The structure is found in a continuous area of Cambro-Silurian sedimentary rocks located in the triangle between Omberg in the south-west, the lake Roxen in east and Karlsdal in north-west (Fig. 3.1). The triangle is submerged into an extended belt of igneous rocks ranging from the east coast in Småland to the north-west, disappearing under the Caledonian mountain range, called the Transscandinavian Igneous Belt (TIB). The TIB is predominated by granites and porphyry but also mafic rocks like gabbro and diorite are present in small volumes.

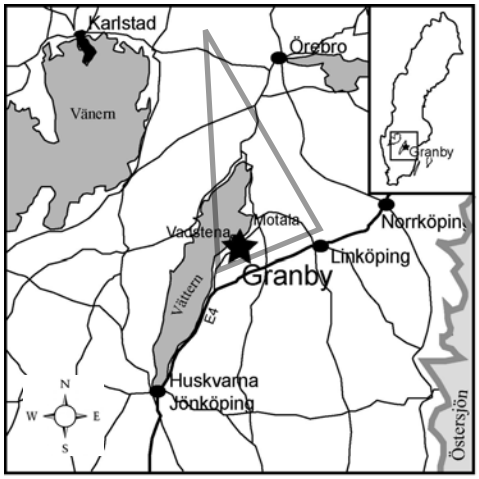

Fig 3.1. Location of the Granby structure in Sweden. Granby is marked with a star. Grey triangle marks the area of Cambro-Silurian sedimentary rocks.

The structure was first described and interpreted by Thorslund (1960) as a diapiric body of granite that had penetrated the sedimentary sequence of strata. Later mapping (Wikman et al. 1982) supplemented these observations with data from well and core drillings as well as some geophysical surveys. This showed that the structure differs substantially from a massive body of crystalline basement. It was found that the basement in fact was located lower in the central parts of the structure, down to approximately 270 meters below the surrounding basement level, and that surrounding this trough the basement was elevated, up to 70 meters above the surrounding basement level (Fig. 3.2). Further, the basement below the bowl shaped structure was found to be brecciated. This clearly indicates that the structure is the result of a high velocity impact. Boreholes in the north-west show that a wide body of igneous rock exists approximately 20 meters below surface and it is given a width of approx. 1 km. This has given the structure an oval shape, which does not correspond well with an impact structure, unless the impact was very oblique.
The impact probably occurred in a shallow ocean (Lindström et al. 2000). Seemingly small movements of water after the impact suggest that the water was slightly shallower than the rim, i.e. less than 100 meter. However, it caused landslides and mud-flows to partly fill the

crater (Lindström et al. 2000). The sequence of rocks filling the crater is described in Wikman et al. 1982, based on the drillings mentioned above and shown in Fig.3.2. The crater is filled by sedimentary rocks of Ordovician age. Deepest lies a sedimentary breccia with fragments of sandstone (lower Cambrian), shale (middle Cambrian), alum shale (probably both middle and upper Cambrian), limestone (lower Ordovician) and fragments of the basement in the area.

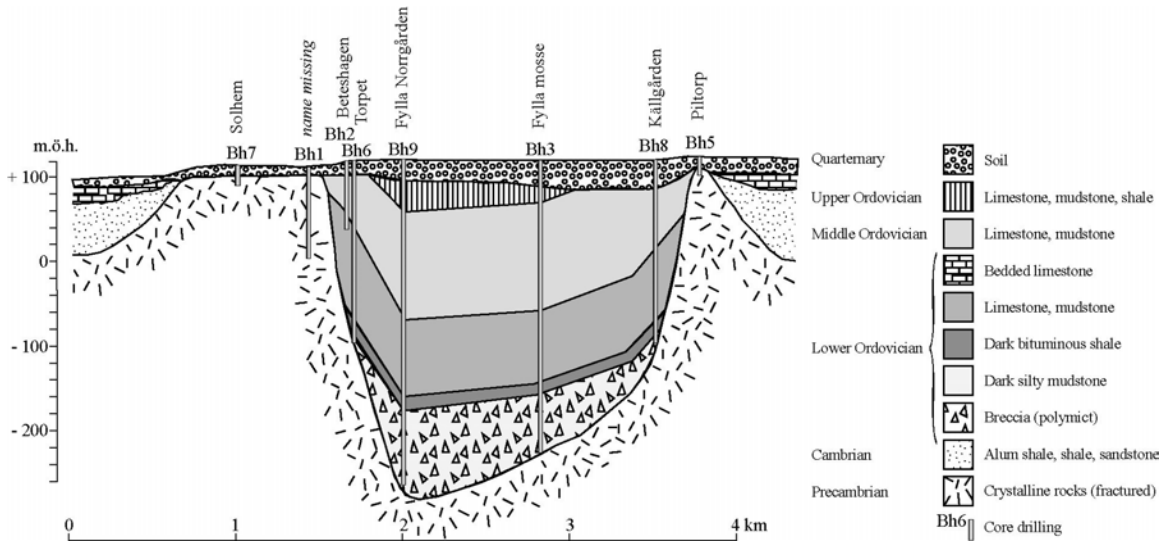

Fig. 3.2. Schematic cross section of the Granby structure. The cross section stretches from NW to SE close to the profile G1 (Fig.4.1). For exact positions of the core drillings and the profile see Wikman, Bruun et al. 1982. Note that the height scale is exaggerated (From Wikman, Bruun et al. 1982).

The matrix consists of a dark clayey and silty (with well rounded quartz) sediment. The fragments are larger in the deeper parts than higher up. The total measured thickness of the breccia is 70 m. Overlying the breccia is a thin (20 m) layer of black bituminous shale,, which seems to be a continuation of the matrix below but without fragments or silt. Overlying the shale is a greenish gray mudstone with high content of lime and thin layers of gray limestone. The distinct boundary between the shale and the following limestone/mudstone indicates movements in the crust at this stage. This material was gradually reduced higher up in the succession and a more ordinary limestone was deposited. The so far presented succession belongs to the Kunda stage (lower Ordovician) and constitutes a thickness of 170 meters, which exceeds other layers of the same age with 150 meters. On top another red-brown limestone of middle Ordovician age follows. It is not possible to clearly distinguish the boundary between these two. Overlying the middle Ordovician rocks are layers of light gray to grayish-green limestone and darker mudstone. The mudstone occurs in far thicker layers than in the surroundings and is the main cause for the middle Ordovician layers to be approx. 60 meters thicker within the crater. Also a layer of bentonite, that is found in the surroundings with a thickness of 1,5 meter, is as thick as 3,5 meter in the center of the crater. The limestone can stratigrafically be compared to the Kullberga limestone in Dalarna, Sweden. The upper Ordovician sequences starts with a limestone and consists further of shale and mudstones. The sequence is very similar to the equivalent layers in the surrounding areas. The youngest layers are probably equivalent to the Dalmanitina layers (upper Ordovician) or the lowest parts of Silurian.

Based on the youngest fragments in the sedimentary breccia the impact most probably occurred in the latest parts of Lanna-Volhov (Volkhov in some literature) stage or earliest part of Kunda stage, in the boundary between Arenig and Llanvirn, some 470 Ma ago. Further some temporarily exposed rock surfaces at Kvarnbacken, close to the crater, showed that the Lanna-Volhov limestone is tilted some 20-40° and even recumbent, i.e. tilted more than 90° (Wikman et al. 1982). At Kvarnbacken a limestone breccia was found with fragments from Lanna-Volhov. According to Wickman (1988) K-Ar dating of a sample of the shale overlying the sedimentary breccia inside the crater gave an age of 472 Ma.

The drillings also show that the structure has been deformed in post Ordovician time, as well as in early Ordovician (boundary between shale and limestone/mudstone mentioned above), indicated by a tilt of the layers by 25-30°. The fact that the shale is found at different depths in different parts of the structure indicates that a submergence of the central parts may have occurred. It may also be a result of slumps or gravitational collapse of the crater wall.

The rim-to-floor depth of simple craters is generally one-third to one-fifth of the rim-to-rim diameter and the rim height is about 4 percent of the diameter according to Melosh (1989). If Granby is about approximated to 2 km wide and has a rim-to-floor depth of almost 380 meters it gives a ratio of 0.19, close to one-fifth. Four percent of 2000 meters is 80 meters, which would indicate that the crater is little or no eroded at all. However, the flat surface of the north-western part of the rim indicates some erosion.

4 Geophysical measurements

4.1 Gravity

The Granby structure was gravimetrically measured between Feb. 18th and Feb. 21st in 2003. The gravimeter used was a LaCoste-Romberg (L788, SGU). The base station, named VAD1 (ID: COCN6901, Appendix 1) at the STF Youth hostel in Vadstena (description Appendix 2), was tied to a fix point named 8117 Motala square 8F (ID: COCN8108, Appendix 1). The area was covered by a net of totally 87 readings (ID: COCN_1 – 87, Appendix 1), 500 to 1000 m apart, in a circular area covering the igneous ring seen at the geological map and extending about 1,5 km outside this ring (Fig 4.1) (co-ordinates Appendix 1). Each day was started and ended by measuring the base station (VAD 1). The gravimeter was put on roads or where there was enough snow to create a close to flat surface, on a plate on the thin snow cover. The gravity values are given in µgal.

About once every hour (ranged between half an hour to at the most two hours) the altitude was measured at known points given by the topographic map. The altitude was determined by measurements with two barometers. Since the markings for the reference points in almost all cases was impossible to find, their location had to be approximated. The heights were later compared with the topographic map and seemed to be rather accurate, within a couple of meters or better. The weather was the whole time dominated by a stable high pressure, sun and no wind. The temperature was about 0 degrees Celsius.

Measurements over the Granby structure

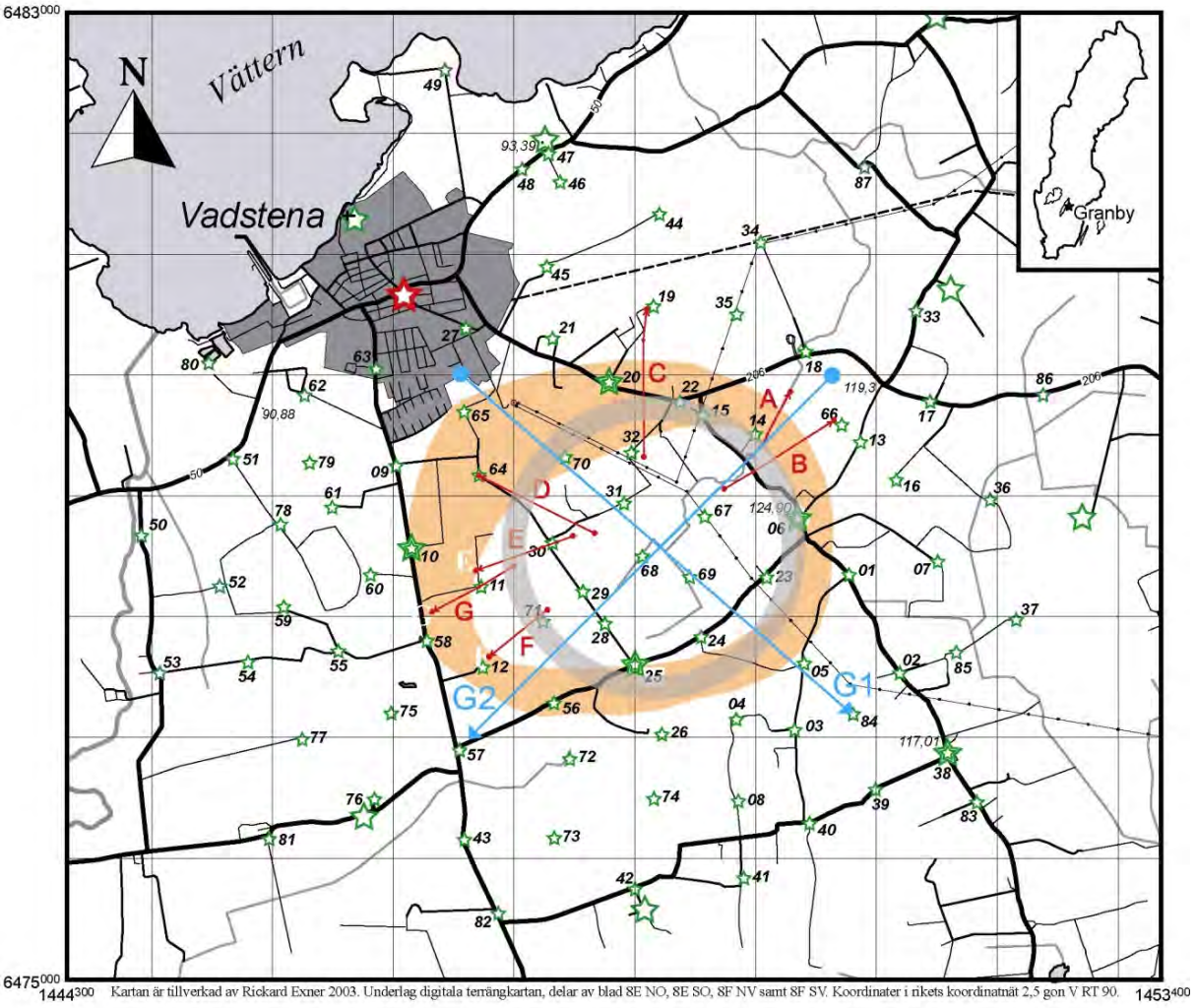

Fig. 4.1. The map shows the 87 gravity measurements (green stars), the seven magnetic profiles (red lines) and the two gravity profiles (blue lines). The grey ring is the placement of the rim of the crater as it is approximated after modeling and analyzing the magnetic profiles. The orange formation is the ring of igneous rocks given in the map of solid rocks (Wikman et al. 1982)

To locate the readings a hand held GPS was used and co-ordinates were obtained in the Swedish grid (RT 90), with 1 m nominal resolution. The spatial accuracy is 10-20 m.

All corrections mentioned earlier were calculated by SGU and the result was presented back as terrain corrected Bouguer gravity. Besides the 87 measurements, 35 points measured earlier were added (Appendix 1). The gravity anomalies are presented as a contour map (Fig. 6.2). There is a regional field in the area with an increase in gravity towards north-west. To compensate for this regional field, a residual separation was made by reducing the field with an inclined plane of similar orientation and opposite sign. A plane was created with negative values in the north-west corner and positive in the south-east. The values were as large as the values in the initial field but of opposite sign to reduce the two corners to zero. In this way the whole area was leveled out and the regional field was roughly reduced. The separation helps to isolate the crater's effect on the gravity field, and to reduce the surrounding field enough to get two profiles for modeling. These two profiles were sliced out with the software Surfer and put into the modeling software GMM (see chapt.5.). Surfer picks the points closest to the chosen path of slicing. Hence, the points are not evenly distributed along the profile as can be seen in the models in chapter 5.1, fig. 5.2b and 5.2c.

The anomalies in the whole area were in the range of 100 gu and in the structure itself about 20 gu.

4.2 Density data

No density data were available for the rocks in the investigated area. Searching through the literature gave no result either. However twenty densities for limestones and three for sandstones from Dalarna of similar age (see chapt. 3.1) were supplied by SGU (Appendix 3), and these showed an average density of 2.681 Mg m^{-3} for the limestone and 2.449 Mgm^{-3} for the sandstone. The mode gave values of 2.69 Mg m^{-3} and 2.455 Mg m^{-3} respectively. In the modeling, a density for the limestones filling the crater of 2.68 Mg m^{-3} seemed adequate. Outside the crater the limestone is overlying a mix of alum shale, shale and sandstone of Cambrian age and a density of 2.59 Mg m^{-3} seemed adequate. Thus, the densities, estimated for the different bodies, are within probable limits.

For the brecciated basement, the density was worked out during modeling (see chapt. 5.1) by testing different values and number of layers. The density is of course lowered by the greatly increased frequency of fractures but since these, in Granby, could be filled mainly with calcite it does not necessary have to mean such a large reduction of density. The final model shows a reduced density of down to –0.4 Mg m^{-3} closest to the crater. This corresponds, assuming that the solid rock has a density of 2.67 Mg m^{-3}, to a density of 2.27 Mg m^{-3} for the most brecciated basement. Broberg (1988) suggests a density for the crushed basement under the Siljan structure down to 2.16 Mg m^{-3}, which would correspond to a porosity of 20%. Assuming that the impact effect on the basement is somewhat smaller in Granby and that the fractures are filled with calcite the modeled density is probable.

There is a possibility that the mixed breccia filling the crater has a lower density and the basement breccia a slightly higher. Rock physical properties of the craters of Dellen (15 km diameter, Sweden), Lappajärvi (23 km diameter, Finland) and Jänisjärvi (14 km diameter, Karelia) show an average breccia density of just over 2.40 Mgm^{-3} (2.42, 2.38, 2.48 Mgm^{-3} respectively) (Henkel, 1992). Densities as low as 2.23 Mgm^{-3} for suevite is indicated in the same table by Henkel (1992). However voluminous melt sheets seems to be restricted to simple, flat-floored impacts with a diameter of over 5 km (Henkel, 1992) so it is unlikely that Granby holds any melt sheet. No such sheet is found in the bore holes. Later work, however, show that slightly higher densities would be more probable (Törnberg et al., 2005).

4.3 Magnetism

To find the rim of the crater and to define its width, magnetic measurements were made using a ground proton precession magnetometer. A magnetic map based on airborne surveys carried out by SGU showed magnetic highs on the southern, south-eastern and north-north-eastern parts of the supposed rim. To fill in the blanks seven ground magnetic profiles were measured in the eastern, northern and western parts (Figure 4.2) of the rim. They were measured in March 2003. Readings were made approximately every 10 metro and the first location was used as base by returning to that point and reading it again. Thus no common base for all the profiles was used. To decide where to put the profiles a circle was drawn on the magnetic map aligning all peaks thought to indicate the rim. The profiles were located across this circle in areas where indications were missing or weak. As the crystalline rocks usually are more magnetic compared to sedimentary rocks, a reduced distance (less sedimentary layer thickness) would result in a positive anomaly. The results of all profiles are shown in Appendix 4.

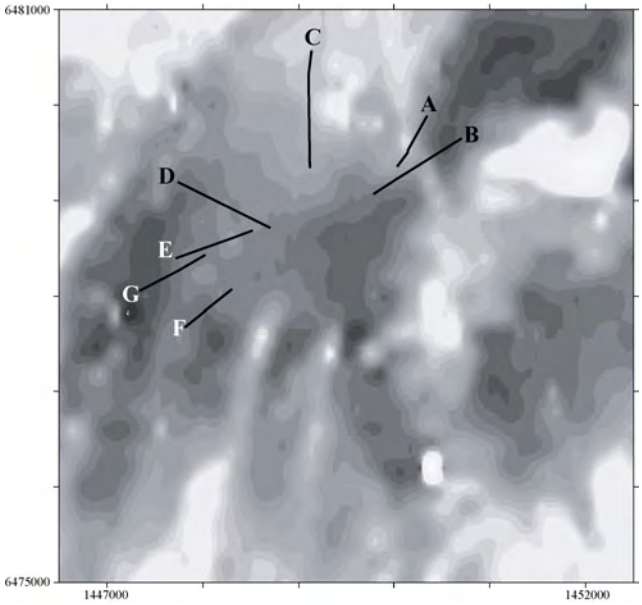

Fig.4.2. Magnetic contour map with high values of magnetism in white and low in black. The seven measured profiles are drawn with black lines. Profile C and F are used for modeling.

4.4 Susceptibility data

Magnetic susceptibilities were measured on cores from SGU's drillings in the 70's (Appendix 6). The sedimentary rocks showed close to no susceptibility at all, as suspected. The brecciated basement gave readings between 0 and $80*10^{-5}$ SI units. After plotting them in a histogram a mode of $1,6*10^{-4}$ SI was obtained.

5 Modeling

The software used, GMM, produced by Geo Vista (1994), is a 2.5 dimensional modeling program for gravity and magnetic data. It can read up to 300 data points and may consist of

up to 20 individual bodies. In the “2.5 dimensional body geometry” the edges of the bodies in perpendicular to the strike direction are vertical but the bodies may be at an arbitrary angle to the profile and be offset sideways, even outside the profile. The bodies may have any strike length. The software requires an IBM PC/AT or compatible computer with a minimum of 540 Kbytes of free RAM, a VGA, EGA or CGA and a math co-processor operating with DOS 2.10 or later versions. The gravity anomalies are presented in gu and the magnetic anomalies in nT.

The gravity was modelled for two profiles ranging from north-west to south-east (G1) and north-east to south-west (G2). The magnetic anomalies were modelled for two profiles over the supposed crater rim in the north (C) and south-west (F) to decide the extent of the crater.

5.1 Gravity modeling

The two profiles G1 and G2 (Fig. 5.1) are 4.2 km long and stretch more or less over the supposed centre of the crater (Fig. 4.1). The surrounding density is set to 2.67 Mg m^{-3}. The regional field is set to –32,4 gu in both models.

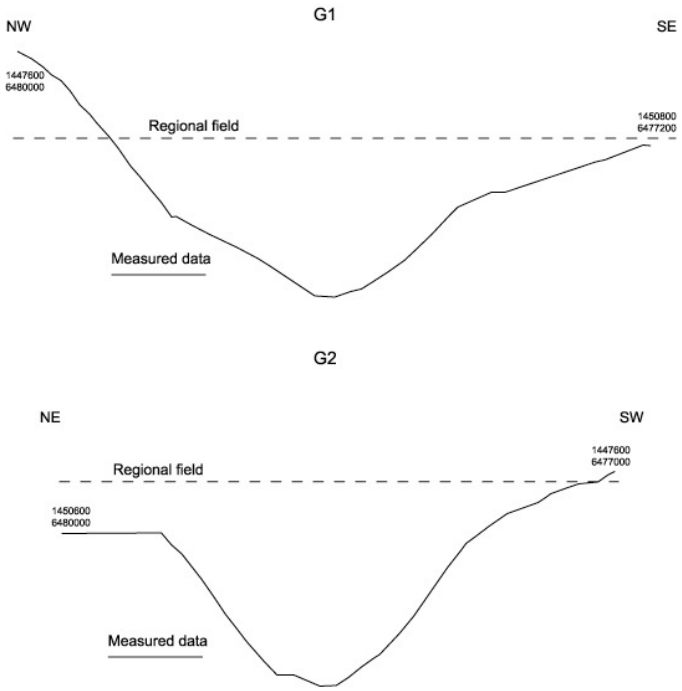

Fig. 5.1. The two profiles, G1 and G2, modeled in GMM (location shown in Fig. 3.1and 5.4). The start and end co-ordinates of the profiles are in the Swedish grid. The

The starting model is a simple crater with width, depth and distribution of filling material, sedimentary rocks and brecciated material according to the cross section in the description to the geological map shown in Fig. 3.2 (Wikman et al. 1982). This cross section is based on drillings performed in the late 70s by SGU. The width of the crater was set to 2 km and the depth to 370 meters below the present rock surface according to the cross section. The brecciated basement is set to almost 3 km wide and 1,5 km deep and divided into six layers with decreasing density towards the centre (the models are shown in Fig. 5.2b and c). Profile G2 is not as deep as G1 as the crater seems to be somewhat irregular and the deepest part is placed close to the north-western or northern side. The same densities are used in both models. In both profiles there are bodies creating gravity anomalies outside the crater and there may also be a remaining effect of the regional field in combination with these. In model G2 a fictional body is put to the right (SW) of the crater to show that it is possible and probable that the curve is influenced by this unknown body. Otherwise no further notice has been taken to this problem since there isn’t enough information of the surroundings.

A problem with the modeling is the unknown densities of the rocks involved (see chapt. 4.2). For the basement the normally used density of 2.67 Mg m^{-3} has been used and the decrease of density in the brecciated basement is decided by testing in the model within reasonable limits. It decreases exponentially outwards from the crater and the values are from the central body and outwards (B1 – B6) set to 2.17, 2.27, 2.44, 2.52, 2.64 respectively 2.665 Mg m^{-3}. This decrease is meant to correspond to the decrease of energy brecciating the rock (see chapter 1.2). The densities of this autogenic[1)] breccia seems to be pretty low but not unlikely (see chapt. 4.2). The allogenic[2)] breccia inside the crater (F3) has been given a slightly lower density compared to the surrounding basement (2.66 Mg m^{-3}). It is a mix of basement rock and Palaeozoic rocks (see chapter 3) with a matrix composed of dark clay, quartz and to some extent pyrite. There is a possibility that the allogenic breccia has a lower density than used in the model and that the autogenic breccia has a slightly higher.

The density of the crater filling (F2), mainly limestones, has been assumed to be similar to densities of rocks of the same age in Dalarna (see chapt.4.2) and has been given a value of 2.68 Mgm^{-3}. Since no real densities are known no effort has been given to divide the different rock types in the succession, nor inside or outside the structure, except for the small body of Upper Ordovician limestone, mudstone and shale (F1). This has been given a higher density of 2.70 Mgm^{-3} for one reason only, to try to adjust the curve to the slight rise or convexitivity existing in the profile (Fig. 5.1). The Lower Ordovician bedded limestone (thin layer) together with the Cambrian mix of alum shale, shale and sandstone, making up the exterior undisturbed sedimentary sequence (S1 & S2), has been given a density of 2.59 Mgm^{-3}. All densities are more or less set to give a probable image of the structure that match the measured anomaly and are not unlikely for the rock types in question. A compilation of the properties of the bodies is presented in Fig. 5.2a.

Fig 5.2a. Table of properties for the bodies in the gravitational models.

	G1			**G2**	
Body	Density (Mgm^{-3})	y-length (m)	Body	Density (Mgm^{-3})	y-length (m)
F1	2.70	1000	F1	2.70	630
F2	2.68	2140	F2	2.68	2230
F3	2.66	1375	F3	2.66	1565
B1	2.17	400	B1	2.17	400
B2	2.27	670	B2	2.27	830
B3	2.44	1150	B3	2.44	1240
B4	2.52	1720	B4	2.52	1700
B5	2.64	2270	B5	2.64	2320
B6	2.665	2750	B6	2.665	2900
S1	2.59	2250	S1	2.59	2250
S2	2.59	2250	S2	2.59	2250
			X	2.64	2540

Fig. 5.2b show the model for profile G1 and Fig. 5.2c the model for G2 (for location, see picture 4.1). White colour is unaffected basement. Dark grey through yellow are the brecciated basement bodies B1–B6 mentioned above. The light grey, light blue and magenta represents the crater filling sediments F1-F3. Brown colours at the sides marked with S1 and

[1)] Autogenic= materials that formed in the rock of, which they are a part during, or soon after, its deposit.
[2)] Allogenic= materials that have been derived from pre-existing rocks and transported some distance to form part of the present unit.

S2 are the exterior sedimentary cover. In model G2 a grey body to the right (X) simulates the rise in gravity due to some unknown reason.

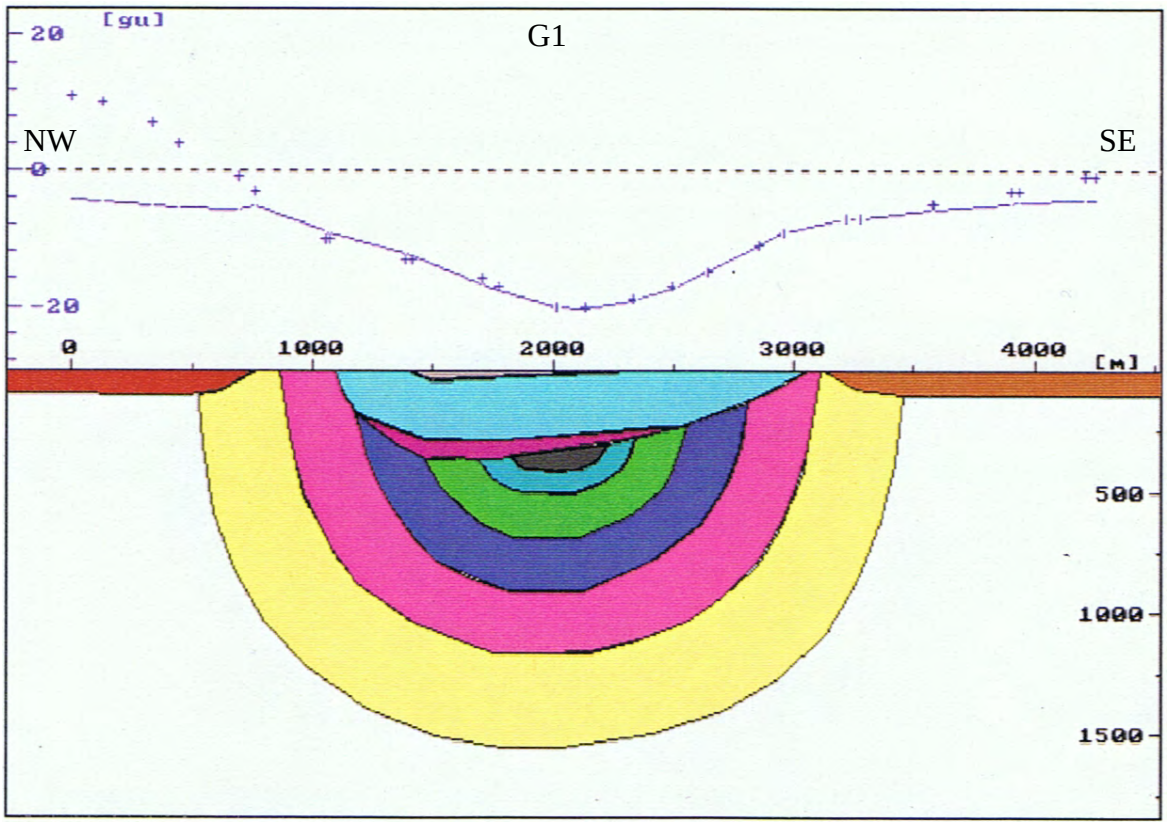

Fig. 5.2b, showing the gravity model for profile G1.

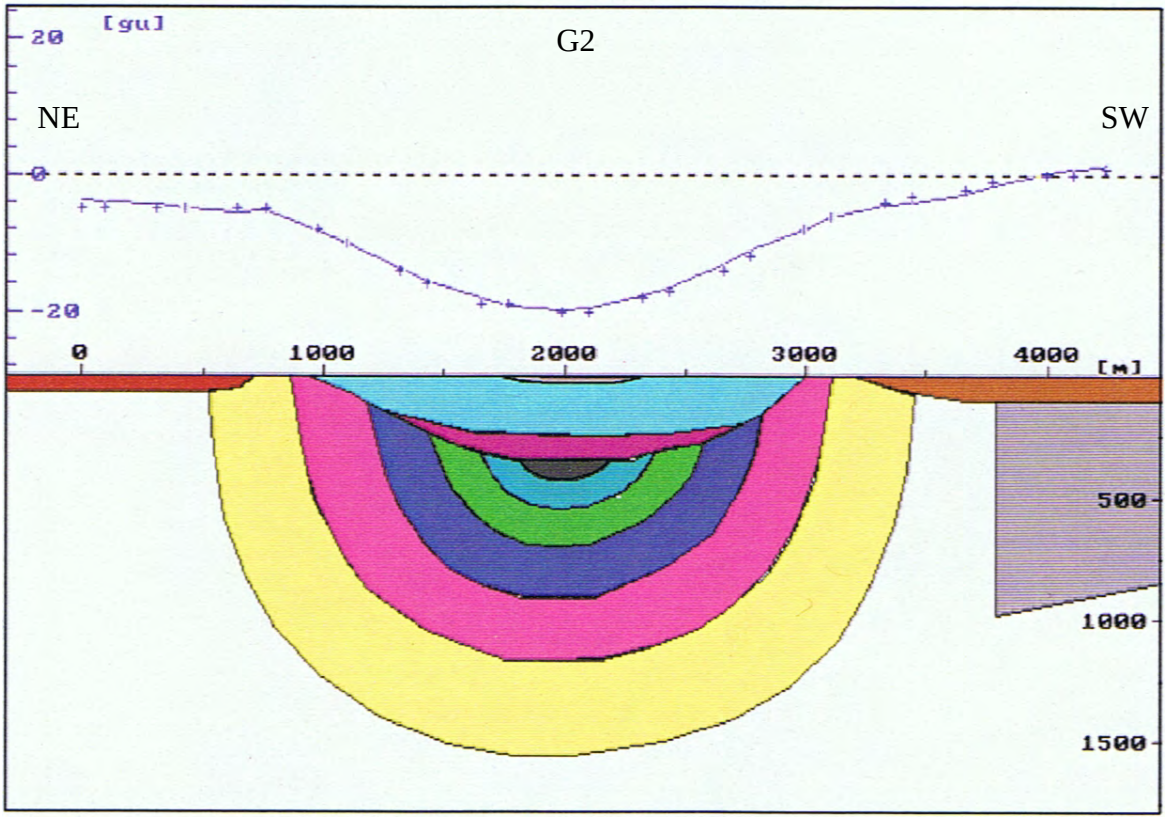

Fig. 5.2c, showing the gravity model for profile G2.

5.2 Magnetic modeling

Two profiles, C and F, of the seven measured have been used for modeling (Appendix 4 & 5). Profile C and F was given a regional magnetic field of 50 235 nT and 50 195 nT respectively. The unaffected basement was given a susceptibility of 0.0027 SI units and the following bodies towards the centre of the crater 0.0026, 0.0016, 0.0012 and 0.0008 SI respectively. The susceptibilities measured on the cores BH 2, 3, 5, 7 and 8 (Appendix 6) show a maximum value of 0.0008 SI. However, modeling showed that these values had to be too small and higher values, within reason, was tried. Typical rock physical properties (Henkel 1991) for crystalline shield rocks of the Baltic shield show that susceptibilities are concentrated between 10^{-1} to 10^{-4} SI. Thus, a value of 0.0027 SI for the unaffected basement seems reasonable. The exterior sedimentary cover was given negative susceptibilities, -0.0006 SI, to create the proper gradient of the peaks. Profile C stretches over an area with higher magnetism than profile F and has therefore been given higher regional field. The reason to these differences in magnetism is unknown since the basement is buried under tens to hundreds of meters of sedimentary rocks. Probable cause is differences in magnetism of the basement due to differences in composition of the rock. Whatever the cause may be it has been compensated for by the difference in regional field.

In profile C (Fig. 5.3a) the rim is marked by a positive anomaly of approximately 20 nT (compared to the surroundings) followed by a decrease towards the centre of the crater (to the left in Fig. 5.3a). The decrease is not even but has a small step about 200-250 meters from the main peak. There is also another positive anomaly some 200-250 m to the right of the main anomaly. This could be the outer limit of the rim. Hence, the model places the rim of the crater between approx. 250 meters and 750 meters from the start of the profile. It is probable that at the most one of the smaller anomalies is associated with the rim and of the two the left one fits best compared with other indicators (Fig. 6.1a) and have been used in the model (Appendix 5). The curve decreases inwards partly due to the decrease of susceptibility, associated with the increase in brecciation and related oxidation of the magnetic components (see chapter 2.2), and partly due to the increasing depth to the magnetic bedrock.

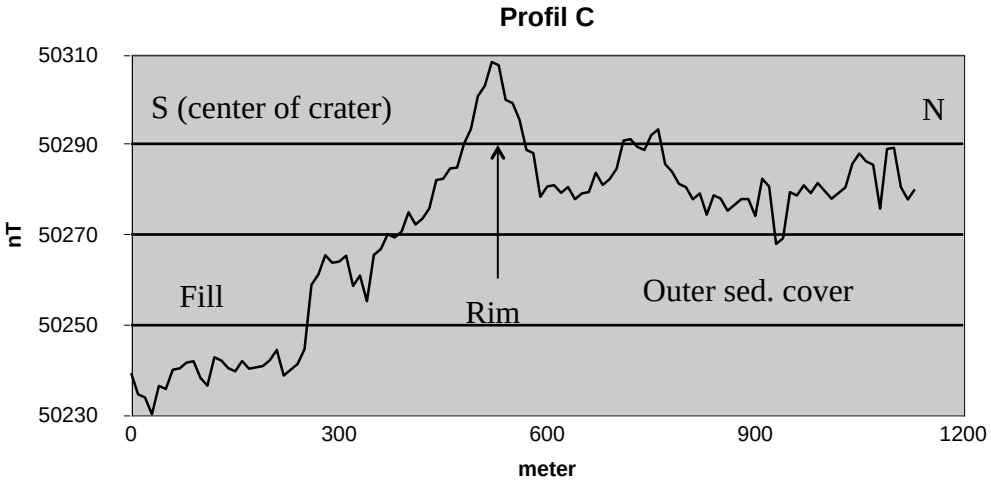

Fig 5.3a, showing the magnetic profile C.

Profile F (Fig. 5.3b) shows a rather smooth and simple curve with a peak of about 30 nT. The negative anomaly on the outside may indicate a trough due to faulting or be an effect of a small water stream that was passed in this section. The model (Appendix 5) places the rim of the crater between approx. 0 and 300 meters from the start of the profile.

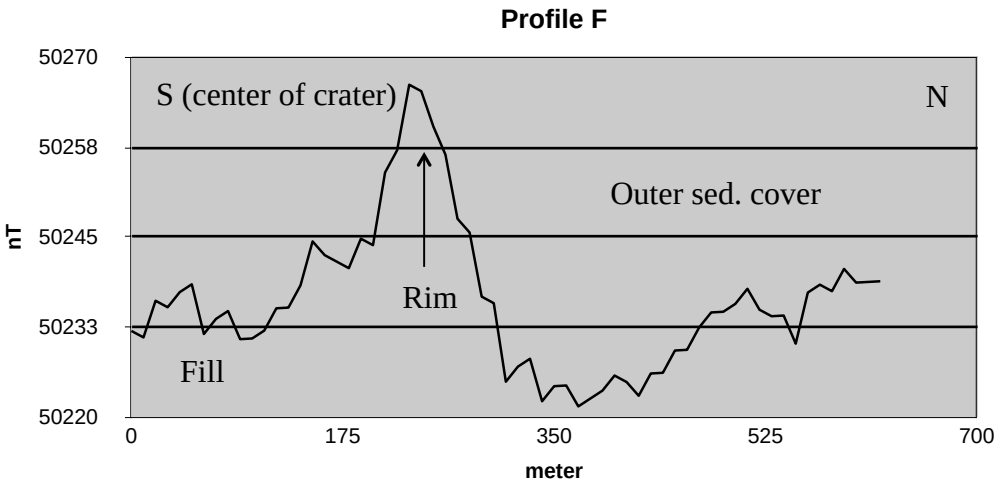

Fig. 5.3b, showing the magnetic profile F.

In profile A (Appendix 4) a peak is visible. However, the peak is very broad and the profile is very irregular and also shows a higher magnetism inside the crater. The magnetic map (Fig. 4.2) shows that the profile is placed on the edge of the more magnetic body reaching from north-east, which may cause the problems. It also seems likely that the profile starts within the rim, which of course complicates the model a lot. Modeling was attempted but not successful.

Profile B (Appendix 4) shows two large positive anomalies at 400 and 600 m from the starting position of the profile and one smaller at 250 m. There is probably a couple of dolerite sills cutting in an oblique angle through this profile, hence creating the two peaks at 400 and 600 m (Appendix 4), which has much larger anomalies of up to 80 nT. The small peak to the left of these “dolerite peaks” could indicate the crater rim but it is much smaller than the anomalies in profile C and F. It places the rim in the vicinity of the estimated position but if the peak marks the outer part of the rim, as it does in profile C and F, the rim will be inside the ring (i.e. the estimated crater rim, see fig 4.1). One probable cause for the peak is the road that cuts through the profile, visible in Fig. 4.1. Another possibility is that the rim is located in direct vicinity to the dolerite sills,, which complicates the modeling severely. This would however place the rim within the circle at a better position than the small peak indicates. This position also corresponds better to the other anomalies visible in the map. An attempt to model according to this scenario did however not yield a satisfying result, and therefore this model was also discarded.

Profile D is very irregular and has no clear anomaly at all. Perhaps the rim could be located somewhere between 100 and 500 m from the starting position. There is no clear decrease towards the centre (to the left), which makes it hard to decide if the slight rise visible between 100 and 500 m in fact is an anomaly that may indicate a rim or if it is a continuous high level

of magnetism that reaches into the crater for some reason. No attempts of modeling this profile were made.

Profile E was strongly disturbed by a farm with large metal cisterns and houses. However, it shows a trend with a peak about 500 meters from the start of the profile. This places the rim close to the ring but as in the case of profile B it would mark the beginning of the rim at this position, which would place the rim inside the circle. The disturbances makes it impossible to decide where a possible peak begins, how big it is or if the anomaly is higher or lower inside the crater compared to outside. Due to this the attempts to model profile E was futile.

Also profile G seems to start on the rim. Further this profile is very irregular and outside the crater it decreases without any visible end. The profile was not modelled because of these problems.

6 Results

The magnetic profiles are indicated on the magnetic map below (Fig. 6.1a and 6.1b) and the rim indications are marked in crossing lines on profiles C and F. They seem to correspond rather well with the other indicators in the magnetic map. The results show an approximately 2 km wide circular structure, which is marked on the figure and also on the map in Fig.4.1. From the indication in the profiles C and F the rim seems most probable to be between 250 and 300 m in width (thickness).

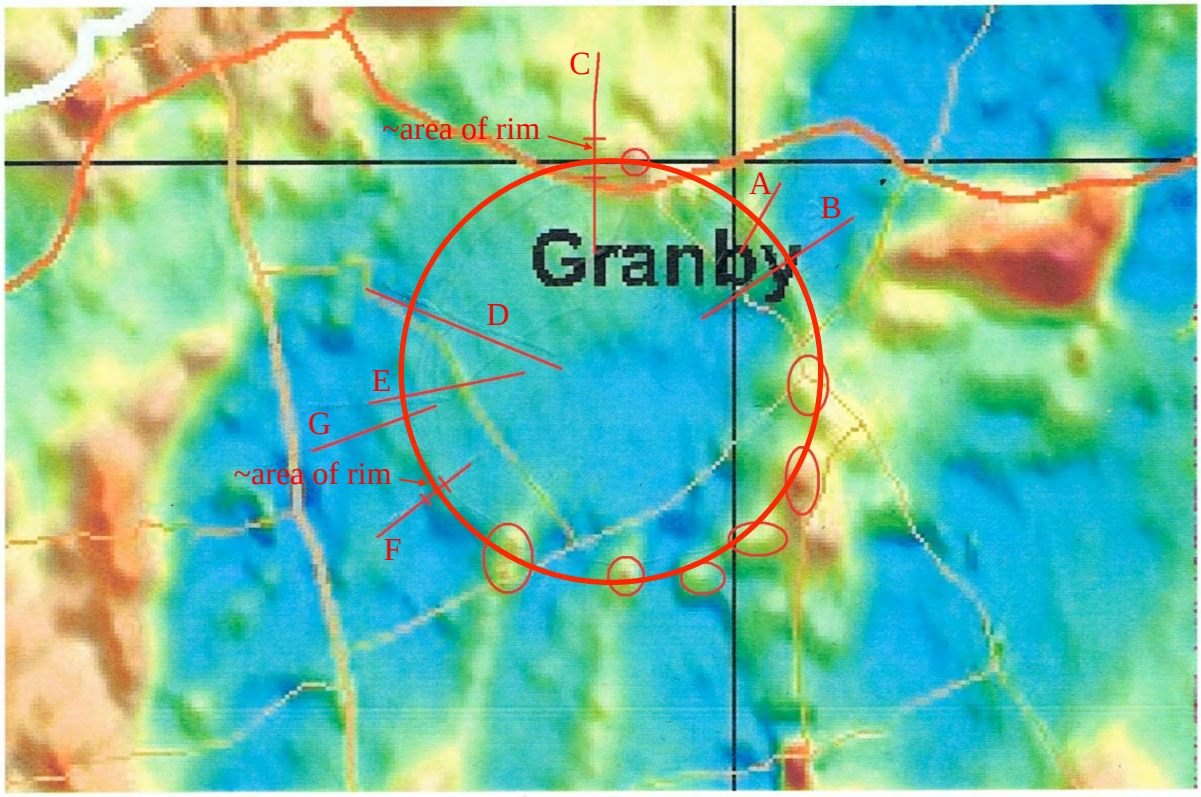

Fig. 6.1a, showing the magnetic map with magnetic profiles and rim indicators. For greater view of area, see Fig. 6.1b on next page.

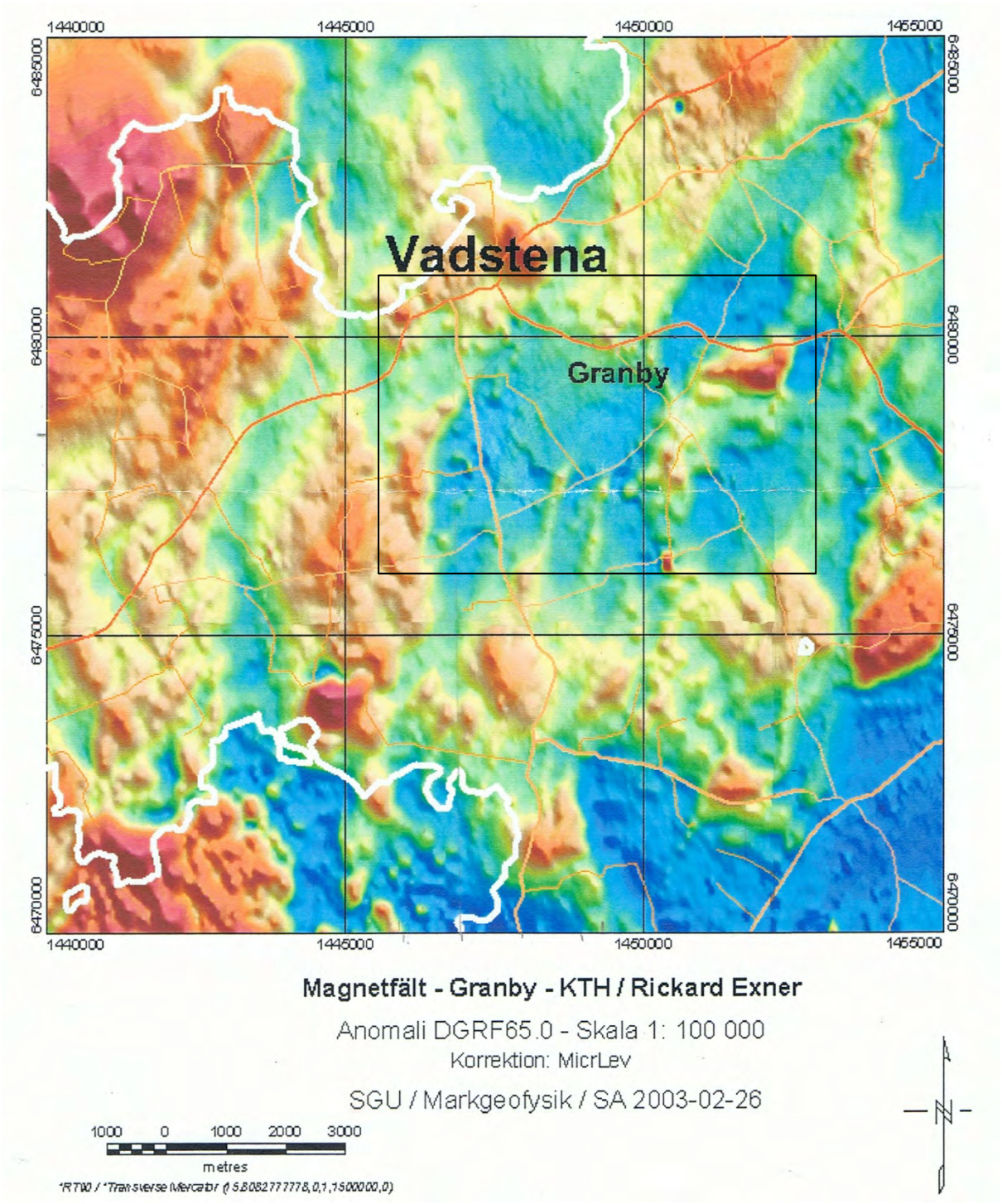

Fig. 6.1b, showing the magnetic map over the area, with the area covered by Fig 6.1a marked with a square in black.

No central uplift is apparent nor in the magnetic map, gravity map or profiles and the structure seems to be a simple crater. The result of the gravimetric survey is shown as a map without the regional correction plane (Fig. 6.2). The correction plane is only a rough estimate of the regional field and mainly used to simplify the modeling.

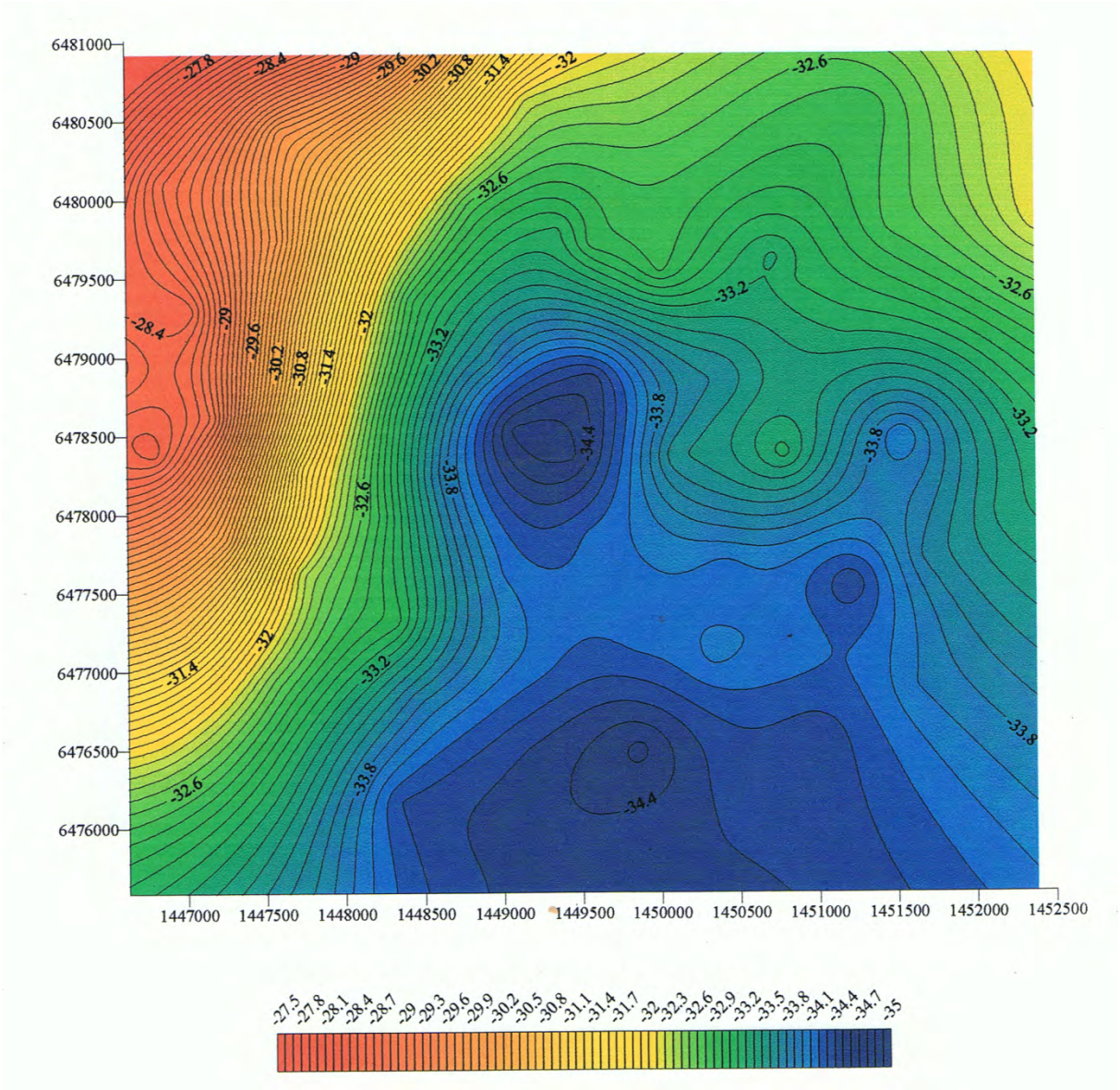

Fig. 6.2 shows the uncorrected gravity map.

The uncorrected map is the achievement of this work and it clearly show that the crater exists and creates a circular and distinct negative anomaly. The crater seems to be only slightly eroded and is well preserved in the Palaeozoic rock sequence.

7 Discussion

The models presented in this work are based on a gravimetric survey over an extensive area compared to the size of the crater. This was done to assure that the gravity effect of the crater was covered completely. With accurate density data on the different layers of Palaeozoic rocks and brecciated as well as homogenous basement, the modeling would maybe be more accurate. However, the main purpose and goal of this survey was to investigate if the gravity anomaly indicated an impact as probable cause of the structure, that is, mainly to see if it is circular in its shape. This goal was achieved. The structure indeed seems to be circular and no central uplift or other feature speaks against the opinion that it is a simple crater. Furthermore, the modeling has given an idea of the possible extension of the brecciation into the basement.

As for the rim of the crater, the gravity model indicates a width of 100 to 400 meters on different sides. The magnetic models both show rims of approximately 250 to 300 meters width. First, the magnetic method is far more sensitive to distance, location, inclination and the azimuth of the actual bodies. Therefore the magnetic models should be seen as a more probable indication of the width of the rim. Second, the gravimetric and magnetic profiles do not coincide and so there may be differences between these areas. The approximated average width of 250 to 300 meters for the rim is thus deemed most probable, but it is most likely to be variable.

The wide area of igneous rock, indicated by two bore holes, mentioned in Wikman et al. (1982) could not be seen in the magnetic map or profiles and unfortunately the magnetic profiles covering this area were not useful for modeling. The disturbed magnetic anomalies may however be a result of this body and it may in fact exist. The outer bore hole (Bh 7) only penetrates the rock 10-20 meters. One possibility is that it is a recumbent part of the basement that overlies the sedimentary rocks below. According to Wikman et al. (1982), there are strongly tilted and even recumbent layers of sedimentary rocks found north-west to the structure and it is also in these parts that an ejected limestone breccia could occur (see chapter 1.3). This may be caused by the impact being oblique, resulting in a larger deposit of ejecta in the downrange direction. This could also create a slightly wider rim at this side (Lindström, personal communication, 2003). This was later also shown to be probable in 3D simulations performed and described by Lindström et al. 2005. The meteorite would in this case scenario have hit from the south-east. The thin layer of basement rock, strongly brecciated, would probably not create any strong gravitational anomaly but most certainly influence the magnetic anomaly. A deeper bore hole in this area could give an answer to this question. Another possible cause could be that a later thrust has created a horst, exposing the Paleozoic rocks to erosion. However, this should clearly be visible as a distinct anomaly of gravitation. The geological map indicates that the structure is oval and, though not as much as indicated there, it may in fact be slightly sub-circular. The G2 model shows a couple of hundred meters wider crater than the G1. This is most probable due to slumps and slides following the cratering process, thus expanding the crater more in the south-west – north-east direction. The shape is very close to circular though and some irregularities are expected.

Further, both the magnetism and gravity in the area is irregular probably due to an irregular top surface along with the difference of composition of the TIB rocks that underlie the Paleozoic sedimentary rocks. Since it is all covered by sedimentary rocks and soil and almost no outcrops can be found, it will not be easy to estimate the effects of variations in magnetism and density within the TIB suite. This makes it hard to decide the normal gravity field in the region and therefore difficult to exactly decide where the anomaly curve is leveled out. I have tried to put the profiles in a right angle to each other, covering the areas where the gravity anomaly is most clearly leveled out outside the structure. This however puts one of them (G1) in a position where it reaches the strong regional anomaly north-west of the structure. Also, the regional field is declining from north-west to south-east. This forced me to create a correctional plane to reduce the measured field, which of course adds uncertainty to the residual anomalies along the G1 profile in particular. However, since the G2 profile is not remarkably influenced, and the two profiles/models seem to correspond well, this correction is considered to be justified.

As for susceptibilities and densities the cores available at SGU could of course be more substantially measured and this would make the models more accurate and easier to create. Densities for the Palaeozoic rocks in Sweden were at the time the modeling was done poorly investigated over. Later work (Törnberg et al. 2005) show that densities estimated in this work seems a bit low.

8 Summary and conclusions

The magnetic profiles are shown on the magnetic map (Fig. 6.1a) and the rim indications are marked with red circles. They seem to correspond well with the other indicators in the magnetic map. A 2 km wide circular structure with a rim of 250 to 300 meters width (thickness) is indicated on Fig. 6.1a and also on the map over the area in Fig. 4.1. No central uplift is apparent neither in the magnetic or gravity map nor in the profiles, and the structure seems to be a simple crater. As result of the gravimetric survey, a map without correction for the regional field is presented (Fig. 6.2). Since a planar correction of the regional field is only a rough estimate of the true regional field, and mainly used to give better profiles for modeling a regional correction was deemed unnecessary. The uncorrected map is the main result of this study, and it clearly shows that the crater exists and creates a circular and distinct negative gravity anomaly of up to 20 gu (μm s^{-2}).

The rim probably reaches between 50 and 100 meters above basement and the crater seems to be only slightly eroded and is well preserved in the Palaeozoic rock sequence. The brecciation of the basement reaches a depth of approx. 1500 meters below the surface and has at lowest, closest to the crater, a density of 2.27 Mgm^{-3}. The impact took place 470 Ma ago in the Lanna-Volhov or Kunda stage.

Although more studies of the structure would be fruitful, the main goal of this work is considered to be achieved, i.e. to measure the gravity anomaly over the structure to create a more detailed gravity map over the area, and to model the structure to establish its main shape and so support the idea that it is an impact crater. The magnetic profiles measured are to be seen as an additional feature to further decide the location of the rim. A magnetic map was

provided by SGU, but in order to complement gaps in some parts it was decided that the presented profiles should be measured. Although the outcome of the magnetic survey may have not have given the desired results, it was possible to place the rim more precisely in two cases.

9 Acknowledgements

The author would like to thank Univ. Lektor Herbert Henkel (KTH) tutor and initiator of this project, for all time and effort put into discussions and the patience he's shown the author; Dr. Sven Aaro (SGU) for supplying facts and research and invaluable advice; Mr. Åke Bruun (SGU) for finding time to supply cores and help; Mr. David Jonhammar, for invaluable field assistance; Lic. Ola Fredin for great computer assistance; Mr. Arne Lif for computer assistance; Student counsellor, manager, undergraduate study administration Mrs. Elisabeth Däcker for believing in me and offering me support in restarting this work; and finally PhD Joakim Mansfeld for great support in helping me finish this work. I also wish to acknowledge the inspiring discussions with the late Prof. Maurits Lindström.

Additional data in table form can be provided by the author.

10 References

Broberg, K.B., 1988, Physical Aspects on Cratering and Slumping in: Deep Drilling in Crystalline Bedrock, Vol. 1, Proceedings of the International Symposium held in Mora and Orsa, Sep. 7-10, 1987, p 261-276, Springer-Verlag berlin Heidelberg.

Geo Vista AB, 1994, GMM Interactive Gravity and Magnetic Modelling Program, User's Manual.

Grieve, R.A.F., 1987, Terrestrial Impact Structures, Ann. Rev. of Earth and Planetary Sci., Vol. 15, p 245-270.

Grive, R.A.F., 1988, The Formation of Large Impact Structures and Constraints on the Nature of Siljan, Deep Drilling in Crystalline Bedrock, Vol. 1, Proceeds of the International Symposium held in Mora and Orsa, Sep. 7-10, 1987, p 328-348, Springer-Verlag berlin Heidelberg.

Henkel, H., 1991, Petrophysical properties (density and magnetization) of rocks from the northern part of the Baltic shield, Tectonophysics, vol.192, p 1-19.

Henkel, H., and Guzmàn, M., 1992, Geophysical Aspects of Meteorite Impact Craters in Eroded Shiel Environment, With Special Emphasis on Electric Resistivity, Tectonophysics, vol. 216, No. 1/2, p 63-90.

Howell, B.F., 1959, Introduction to Geophysics, McGraw-Hill series in the Geological Sciences, McGraw-Hill Book Company, Inc, New York, Toronto, London, 399 pp.

Lindström, M., Lundqvist, J., Lundqvist, T., 2000, Sveriges Geologi från Urtid till Nutid, Second Edition, Studentlitteratur, 491 pp.

Lindström, M., Shuvalov, V., Ivanov, B., 2005, Lockne crater as a result of marine-target oblique impact, Planetary and Space Science 53 (2005) p 803-815.

Melosh, H. J., 1989, Impact Cratering, a geologic press, Oxford University Press, Inc, 245 pp.

Melosh, H.J., Ivanov, B.A., 1999, Impact Crater Collapse, Annual Review of Earth Planet Science 1999, 27, p 385-415.

Milsom, J., 1996, Field Geophysics, second edition, John Wiley & Sons Ltd, England, 187 pp.

Törnberg, R., Sturkell, E.F.F., 2005, Density and magnetic susceptibility of rocks from the Lockne and Tvären marine impact structures, Meteoritics & Planetary Science 40, Nr 4, 639-651 (2005).

Wickman, F.E., 1988, Possible Impact Structures in Sweden, Deep Drilling in Crystalline Bedrock, Vol. 1, Proceeds of the International Symposium held in Mora and Orsa, Sep. 7-10, 1987, p 298-327, Springer-Verlag berlin Heidelberg.

Wikman, H., Bruun, Å., Dahlman, B., Vidal, G., 1982, Beskrivning till berggrundskartan HJO NO, Description to the map of solid rocks HJO NO, Sveriges Geologiska Undersökning, Uppsala, Ser. Af 120.

11 Appendix

Appendix 1 – Table of gravity stations

Y- and x- co-ordinates in column one and two are in Swedish grid RT 90. Boug (col.3) means extended Bouguer gravity (SGU, Lantmäteriverket). Id (col.4) is identification number for the station. H (col.5) is height above sea level as measured. Q (col.6) is the quality of the height value as described below. Tcorr (col.7) is a temperature correction. Map (col.8) is the topographic map covering the station. Lat (col.9) and long (col.10) is co-ordinates in latitude and longitude. Y (col.11) is the year the station was measured.

```
y- och x-coord Boug(IGSN71) id   H   h-qual  tcorr   map  latitud  longitud year
ECS62 to IGSN71: IGSN71=ECS62-14.6-(-16.3+13.7(sin(lat))**2) mGal
 E-W    N-S (Koordinater i Rikets nät, RT38 el RT90, och lat/long enl. Bessel)
h-kval: 1          innebär cm-noggrannhet,  medelfel 0,05 m
        2, 5 och 6    -"-  dm-    -"-    ,  medelfel 0,2 m
        3 och 7       -"-   m-    -"-    ,  medelfel ca 3 m
        8 hojdbest med barometer         ,  medelfel ca 2 m
        B hojdbest med barometer, bra omst, medelfel ca 1 m
        9   -"-     "  sGPS, medelfel ca 0.2 m
        p   -"-     "  sGPS             ,  medelfel 0,2 m
        q   -"-     "  sGPS             ,  medelfel 0,5 m
        r   -"-     "  sGPS             ,  medelfel 1,5 m
        D okorrigerad havsyta som ref, medelfel ca 0,5 m
        H korrigerad havsyta som ref,  medelfel ca 0,1 m
        M interpol fran 1000m x 1000m DTM
        N   -"-          500m x  500m DTM
        L   -"-           50m x   50m DTM
```

y-coord	x-coord	Boug	id	H	q	tcorr	map	lat	long	y
1441270	6471250	-32.130	LMV.4851	97.60	3	-0.01	8E	58 21.66	14 48.29	83
1448040	6473190	-34.736	LMV.4951	113.16	1	0.05	8E	58 22.75	14 55.20	83
1452500	6474370	-35.223	LMV.4051	116.04	1	0.03	8F	58 23.42	14 59.76	83
1449115	6475563	-34.397	RAHQ5915	116.80	q	0.03	8E	58 24.04	14 56.27	00
1441380	6475570	-31.018	LMV.5852	108.44	1	0.01	8E	58 23.99	14 48.34	83
1444990	6476090	-32.584	LMV.5853	102.26	1	0.00	8E	58 24.29	14 52.03	83
1453995	6476264	-32.292	RAHQ5012	107.40	q	0.01	8F	58 24.45	15 1.27	00
1446745	6476372	-32.330	RAHQ5912	110.30	q	0.02	8E	58 24.46	14 53.83	00
1443120	6476700	-30.418	RAHQ5813	104.40	8	0.01	8E	58 24.61	14 50.11	00
1451595	6476841	-34.294	RAHQ5011	114.00	q	0.02	8F	58 24.75	14 58.80	00
1441000	6477250	-29.360	RAHQ5812	117.20	8	0.07	8E	58 24.89	14 47.92	00
1449011	6477615	-33.660	RAHQ5914	124.30	q	0.10	8E	58 25.14	14 56.14	00
1445406	6478228	-29.076	RAHQ5911	93.10	q	-0.02	8E	58 25.45	14 52.43	00
1443142	6478259	-28.616	RAHQ5810	98.40	q	-0.01	8E	58 25.45	14 50.10	00
1454482	6478463	-31.652	RAHQ5013	122.49	p	0.04	8F	58 25.64	15 1.75	00
1447171	6478593	-28.802	RAHQ5913	110.50	q	0.02	8E	58 25.66	14 54.24	00
1452747	6478829	-32.331	RAHQ5010	117.80	q	0.05	8F	58 25.82	14 59.96	00
1450350	6478850	-33.042	LMV.5051	124.90	1	0.06	8F	58 25.82	14 57.50	83
1441410	6479520	-25.469	LMV.5851	123.00	1	0.12	8E	58 26.11	14 48.31	83
1448791	6479931	-32.428	RAHQ5910	111.80	q	0.02	8E	58 26.39	14 55.88	00
1444133	6479985	-25.616	RAHQ5811	90.20	r	-0.02	8E	58 26.39	14 51.10	00
1445730	6480190	-26.558	LMV.6952	90.20	1	-0.02	8E	58 26.51	14 52.73	83
1453735	6480675	-31.297	RAHQ6012	127.10	q	0.06	8F	58 26.82	15 0.95	00
1451673	6480748	-33.036	RAHQ6013	110.20	q	0.02	8F	58 26.85	14 58.83	00
1446680	6481180	-27.126	LMV.6951	96.47	2	0.00	8E	58 27.05	14 53.70	43
1443534	6481763	-22.119	RAHQ6810	89.70	q	-0.02	8E	58 27.34	14 50.46	00
1448260	6481980	-25.927	LMV.6953	93.37	1	-0.01	8E	58 27.49	14 55.31	83
1440140	6482005	-14.030	RAHQ6812	90.20	8	-0.02	8E	58 27.44	14 46.96	00
1441810	6482680	-14.369	LMV.6851	113.30	2	0.11	8E	58 27.82	14 48.67	83
1451560	6483000	-32.337	LMV.6051	128.80	1	0.15	8F	58 28.06	14 58.69	83
1449480	6483052	-29.753	RAHQ6910	91.12	p	-0.01	8E	58 28.08	14 56.55	00
1453560	6483637	-30.879	RAHQ6011	116.40	q	0.03	8F	58 28.42	15 0.74	00
1443000	6484135	-19.619	RAHQ6811	95.40	q	0.01	8E	58 28.61	14 49.87	00
1451987	6484869	-30.854	RAHQ6010	113.72	p	0.05	8F	58 29.07	14 59.10	00
1449382	6484909	-27.280	RAHQ6911	90.37	p	-0.01	8E	58 29.08	14 56.42	00

1447092	6480675	-28.432	COCN6901	98.00	8	0.00	08E	58	26.78	14	54.13	03
1449851	6477171	-34.072	COCN___4	118.80	8	0.02	08E	58	24.91	14	57.01	03
1449864	6476503	-34.533	COCN___8	118.80	8	0.03	08E	58	24.55	14	57.03	03
1447019	6479285	-28.314	COCN___9	103.30	8	0.02	08E	58	26.03	14	54.07	03
1447172	6478598	-28.734	COCN__10	110.50	8	0.03	08E	58	25.66	14	54.24	03
1447723	6478278	-31.567	COCN__11	116.80	8	0.03	08E	58	25.49	14	54.81	03
1447731	6477612	-32.267	COCN__12	117.40	8	0.03	08E	58	25.13	14	54.83	03
1449578	6479715	-32.859	COCN__15	119.00	8	0.04	08E	58	26.28	14	56.69	03
1449160	6480622	-32.210	COCN__19	104.30	8	0.01	08E	58	26.77	14	56.25	03
1448805	6479969	-32.623	COCN__20	110.10	8	0.03	08E	58	26.41	14	55.90	03
1448314	6480349	-30.873	COCN__21	102.40	8	0.01	08E	58	26.61	14	55.39	03
1449377	6479817	-33.102	COCN__22	120.00	8	0.05	08E	58	26.33	14	56.49	03
1449560	6477862	-34.075	COCN__24	122.50	8	0.05	08E	58	25.28	14	56.70	03
1449011	6477620	-34.013	COCN__25	122.80	8	0.04	08E	58	25.15	14	56.14	03
1449220	6477051	-34.043	COCN__26	121.30	8	0.05	08E	58	24.84	14	56.36	03
1447599	6480432	-29.733	COCN__27	98.70	8	0.00	08E	58	26.65	14	54.65	03
1448753	6477961	-33.837	COCN__28	116.60	8	0.02	08E	58	25.33	14	55.87	03
1448570	6478227	-33.639	COCN__29	116.70	8	0.03	08E	58	25.47	14	55.68	03
1448311	6478644	-32.939	COCN__30	121.70	8	0.05	08E	58	25.69	14	55.41	03
1448915	6478968	-33.687	COCN__31	120.70	8	0.04	08E	58	25.87	14	56.02	03
1448970	6479387	-33.357	COCN__32	114.70	8	0.03	08E	58	26.10	14	56.07	03
1449852	6480548	-32.439	COCN__35	105.90	8	0.01	08E	58	26.73	14	56.96	03
1449910	6475858	-34.298	COCN__41	111.50	8	0.02	08E	58	24.20	14	57.09	03
1449007	6475766	-34.318	COCN__42	121.10	8	0.03	08E	58	24.15	14	56.16	03
1447579	6476165	-33.239	COCN__43	114.10	8	0.02	08E	58	24.35	14	54.69	03
1449209	6481384	-31.005	COCN__44	93.10	8	-0.01	08E	58	27.18	14	56.29	03
1448270	6480951	-29.125	COCN__45	99.40	8	0.01	08E	58	26.94	14	55.33	03
1448376	6481656	-27.068	COCN__46	93.30	8	-0.01	08E	58	27.32	14	55.43	03
1448285	6481887	-26.364	COCN__47	92.40	8	-0.01	08E	58	27.44	14	55.34	03
1448069	6481765	-26.247	COCN__48	93.40	8	-0.01	08E	58	27.37	14	55.12	03
1447431	6482584	-24.801	COCN__49	92.10	8	-0.02	08E	58	27.81	14	54.45	03
1444883	6478704	-28.418	COCN__50	91.50	8	-0.02	08E	58	25.70	14	51.89	03
1445657	6479347	-27.277	COCN__51	91.80	8	-0.02	08E	58	26.05	14	52.67	03
1445541	6478286	-28.802	COCN__52	93.30	8	-0.02	08E	58	25.48	14	52.57	03
1445038	6477560	-30.094	COCN__53	97.40	8	-0.01	08E	58	25.09	14	52.06	03
1445785	6477652	-30.018	COCN__54	98.90	8	-0.01	08E	58	25.14	14	52.83	03
1446530	6477747	-29.433	COCN__55	106.00	8	0.02	08E	58	25.20	14	53.59	03
1448328	6477316	-32.952	COCN__56	124.40	8	0.05	08E	58	24.98	14	55.44	03
1447556	6476925	-32.531	COCN__57	120.40	8	0.04	08E	58	24.76	14	54.66	03
1447262	6477826	-30.239	COCN__58	118.20	8	0.04	08E	58	25.25	14	54.34	03
1446080	6478102	-28.585	COCN__59	99.90	8	0.00	08E	58	25.39	14	53.12	03
1446802	6478382	-28.257	COCN__60	103.90	8	0.01	08E	58	25.54	14	53.86	03
1446490	6478942	-28.779	COCN__61	98.80	8	0.00	08E	58	25.84	14	53.53	03
1446248	6479881	-27.787	COCN__62	92.70	8	-0.01	08E	58	26.35	14	53.27	03
1446841	6480104	-28.674	COCN__63	97.10	8	0.00	08E	58	26.47	14	53.88	03
1447709	6479200	-30.594	COCN__64	116.50	8	0.04	08E	58	25.99	14	54.78	03
1447588	6479745	-29.796	COCN__65	110.40	8	0.03	08E	58	26.28	14	54.65	03
1449586	6478856	-34.351	COCN__67	119.30	8	0.02	08E	58	25.82	14	56.71	03
1449065	6478533	-34.510	COCN__68	116.90	8	0.02	08E	58	25.64	14	56.18	03
1449458	6478360	-34.512	COCN__69	115.90	8	0.02	08E	58	25.55	14	56.59	03
1448424	6479358	-32.752	COCN__70	114.40	8	0.03	08E	58	26.08	14	55.51	03
1448243	6477980	-32.834	COCN__71	116.60	8	0.02	08E	58	25.34	14	55.35	03
1448458	6476834	-33.753	COCN__72	110.40	8	0.01	08E	58	24.72	14	55.58	03
1448336	6476175	-34.196	COCN__73	111.10	8	0.01	08E	58	24.36	14	55.47	03
1449156	6476511	-34.297	COCN__74	114.80	8	0.02	08E	58	24.55	14	56.30	03
1446972	6477225	-30.892	COCN__75	105.50	8	0.01	08E	58	24.92	14	54.05	03
1446833	6476511	-32.116	COCN__76	112.20	8	0.02	08E	58	24.53	14	53.92	03
1446237	6477009	-30.967	COCN__77	99.50	8	0.00	08E	58	24.80	14	53.30	03
1446041	6478805	-28.211	COCN__78	97.10	8	-0.01	08E	58	25.76	14	53.07	03
1446292	6479322	-28.203	COCN__79	97.30	8	0.00	08E	58	26.04	14	53.32	03
1445448	6480146	-25.946	COCN__80	89.90	8	-0.02	08E	58	26.48	14	52.45	03
1445952	6476187	-32.483	COCN__81	105.50	8	0.01	08E	58	24.35	14	53.02	03
1447858	6475558	-33.752	COCN__82	109.40	8	0.01	08E	58	24.03	14	54.98	03
1458563	6494713	-25.128	COCN8101	95.90	1	0.09	8F	58	34.42	15	05.76	03
1450787	6478380	-33.152	COCN___1	115.70	8	0.04	8F	58	25.57	14	57.95	03
1451208	6477558	-34.293	COCN___2	112.90	8	0.02	8F	58	25.13	14	58.40	03
1450337	6477096	-33.966	COCN___3	124.90	8	0.06	8F	58	24.87	14	57.51	03
1450415	6477635	-34.063	COCN___5	121.00	8	0.04	8F	58	25.17	14	57.58	03
1450404	6478860	-33.594	COCN___6	124.40	8	0.05	8F	58	25.82	14	57.55	03

1451531	6478488	-33.999	COCN___7	109.90	8	0.02	8F	58	25.63	14	58.72	03
1450891	6479494	-33.079	COCN__13	115.70	8	0.03	8F	58	26.17	14	58.05	03
1450011	6479549	-32.775	COCN__14	113.10	8	0.03	8F	58	26.19	14	57.14	03
1451177	6479169	-33.181	COCN__16	115.80	8	0.07	8F	58	26.00	14	58.34	03
1451467	6479834	-32.672	COCN__17	114.30	8	0.02	8F	58	26.36	14	58.63	03
1450437	6480231	-32.743	COCN__18	111.50	8	0.02	8F	58	26.56	14	57.57	03
1450101	6478363	-33.510	COCN__23	124.00	8	0.05	8F	58	25.56	14	57.25	03
1451354	6480584	-32.755	COCN__33	110.60	8	0.02	8F	58	26.76	14	58.51	03
1450060	6481143	-32.047	COCN__34	101.80	8	0.02	8F	58	27.05	14	57.17	03
1451969	6478995	-33.152	COCN__36	108.60	8	0.01	8F	58	25.91	14	59.16	03
1452183	6477999	-33.348	COCN__37	108.60	8	0.00	8F	58	25.37	14	59.39	03
1451633	6476909	-33.894	COCN__38	116.90	8	0.03	8F	58	24.78	14	58.84	03
1451006	6476585	-34.268	COCN__39	113.80	8	0.02	8F	58	24.60	14	58.20	03
1450457	6476308	-34.244	COCN__40	117.80	8	0.03	8F	58	24.45	14	57.64	03
1450725	6479631	-33.223	COCN__66	110.60	8	0.02	8F	58	26.24	14	57.87	03
1451858	6476482	-33.956	COCN__83	116.40	8	0.03	8F	58	24.55	14	59.08	03
1450827	6477220	-33.995	COCN__84	115.70	8	0.03	8F	58	24.94	14	58.01	03
1451693	6477733	-33.656	COCN__85	111.00	8	0.02	8F	58	25.23	14	58.89	03
1452411	6479878	-32.102	COCN__86	112.50	8	0.02	8F	58	26.39	14	59.60	03
1450912	6481777	-32.009	COCN__87	105.80	8	0.01	8F	58	27.40	14	58.04	03

Appendix 2 – Description of the base station

TYNGDKRAFTSMÄTNING - BASPUNKTSBESKRIVNING
SGU, Box 670, 751 28 UPPSALA, 018-179000

Baspunkt	Område	Gravimeter	Projekt kod
VAD7	Granby / Vadstena	L788	

Anges av LS

Datum	Inmätningssekvens - Se manual (Ex. 1801 - Pustnäs 2 - 1801 eller 1801 - 2401 - Pustnäs 2 - 2401 - 1801 eller Pustnäs 2 - 1801 - Pustnäs 2 etc)	Observatör
030218	VAD7-8117-Vad7	RE

Anmärkning: VAD7 - Baspunkt vid STF enligt skiss nedan 6480676 1447093 h=98

Datum	Inmätningssekvens	Observatör
030221	VAD7 - 8117 - VAD7	

Anmärkning:

Beskrivning - skiss. Punktens läge ska anges så noggrant som möjligt. Målet är att samma punkt ska kunna användas för fortsatta mätningar i området. Ungefärliga avstånd och nordpil ska alltid anges om punkten inte beskrivs med hjälp av fotografier.
Om fixpunkt används som baspunkt klistras del av fixpunktsbeskrivningen i denna ruta.

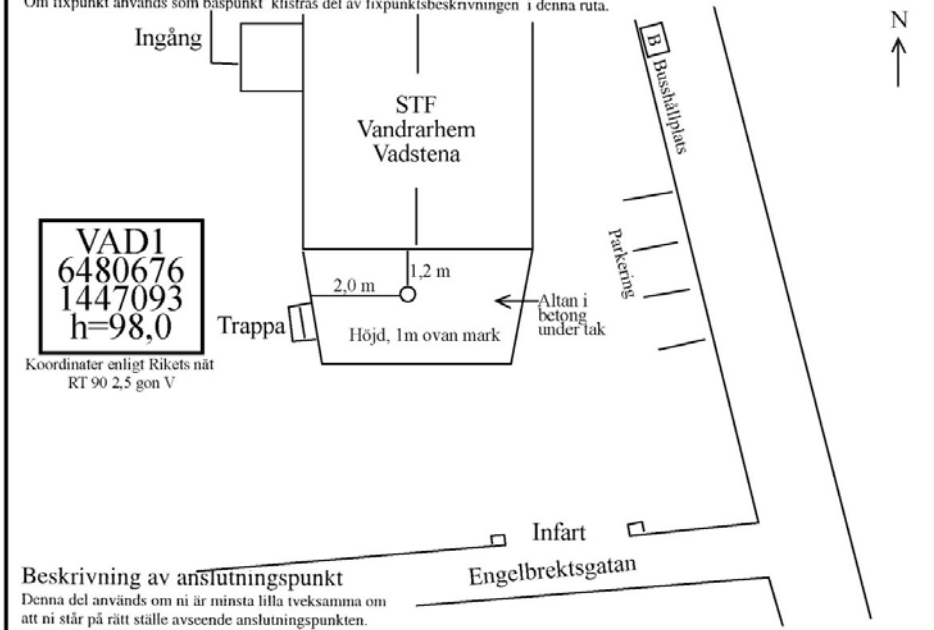

Beskrivning av anslutningspunkt
Denna del används om ni är minsta lilla tveksamma om att ni står på rätt ställe avseende anslutningspunkten.

Anslutningspunkt - 8117 Motala 8F

6494706 1458574
höjd 95,902

Appendix 3 – Densities and susceptibilities for some limestones and sandstones from Dalarna.

Supplied by SGU. PALSA = sandstone, PALSKA = limestones.

/y- och	x-koord	bergk	dens	itet susc	q	dekl	inkl	Id	kbl	obj/geol
1468490	6766850	PALS	2447	0.000026	*	*	*	SA88066	14F	HS
1443800	6785300	PALSA	2436	0.000035	*	*	*	SA88084	14E	HS
1466316	6773966	PALSA	2465	0.000134	1.04	*	*	SS85143	14F	HS
1462350	6781030	PALSKA	2694	0.000034	*	*	*	SA86039	14F	HS
1457460	6755550	PALSKA	2689	0.000144	0.31	*	*	SA86046	14F	HS
1464950	6773800	PALSKA	2690	0.000015	*	*	*	SA89045	14F	H
1425740	6762700	PALSKA	2701	0.000034	*	*	*	SA89055	14E	H
1466150	6777180	PALSKA	2688	0.000030	*	*	*	SA89087	14F	HS
1466607	6773484	PALSKA	2695	0.000031	*	*	*	SS85142	14F	H
1465003	6773727	PALSKA	2684	0.000099	*	*	*	SS85145	14F	H
1464259	6772001	PALSKA	2683	0.000222	0.71	*	*	SS85148	14F	H
1464388	6767135	PALSKA	2668	0.000108	1.35	*	*	SS85155	14F	H
1467852	6769875	PALSKA	2667	0.000096	*	*	*	SS85158	14F	HS
1467424	6770712	PALSKA	2670	0.000056	*	*	*	SS85159	14F	HS
1463399	6762734	PALSKA	2658	0.000115	1.75	*	*	SS85165	14F	HS
1469839	6762952	PALSKA	2685	0.000076	*	*	*	SS85168	14F	H
1468199	6763169	PALSKA	2690	0.000063	*	*	*	SS85169	14F	H
1462137	6759462	PALSKA	2631	0.000103	1.84	*	*	SS85171 A	14F	H
1462137	6759462	PALSKA	2688	0.000146	1.64	*	*	SS85171 B	14F	H
1462137	6759462	PALSKA	2689	0.000155	1.31	*	*	SS85171 C	14F	H
1461516	6758698	PALSKA	2686	0.000098	*	*	*	SS85172 A	14F	H
1461516	6758698	PALSKA	2686	0.000156	1.29	*	*	SS85172 B	14F	H
1461516	6758698	PALSKA	2676	0.000113	1.16	*	*	SS85172 C	14F	H

Medel PALSKA	2680,9	Typvärde PALSKA	2690
Medel PALSA	2449,333	Typvärde PALSA	2455

Appendix 4 – Magnetic profiles

All curves are measured from inside the crater and out. Single point anomaly values are likely to be erratic measurements due to external sources.

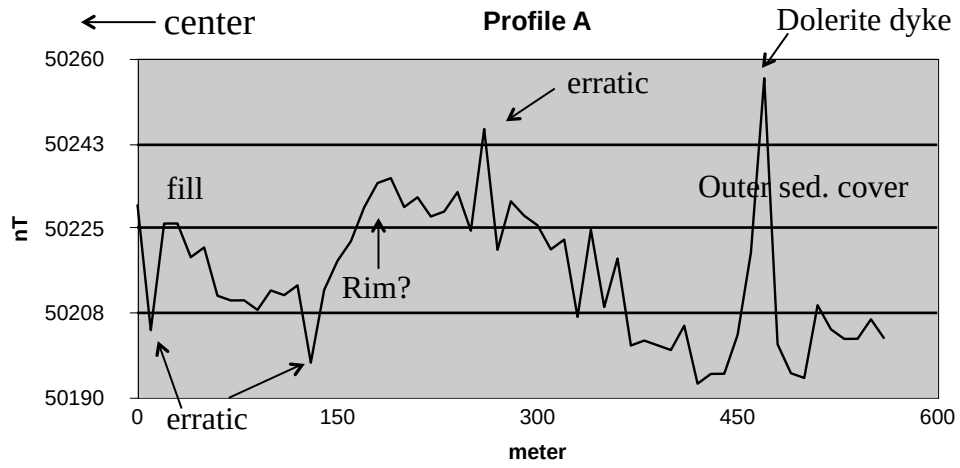

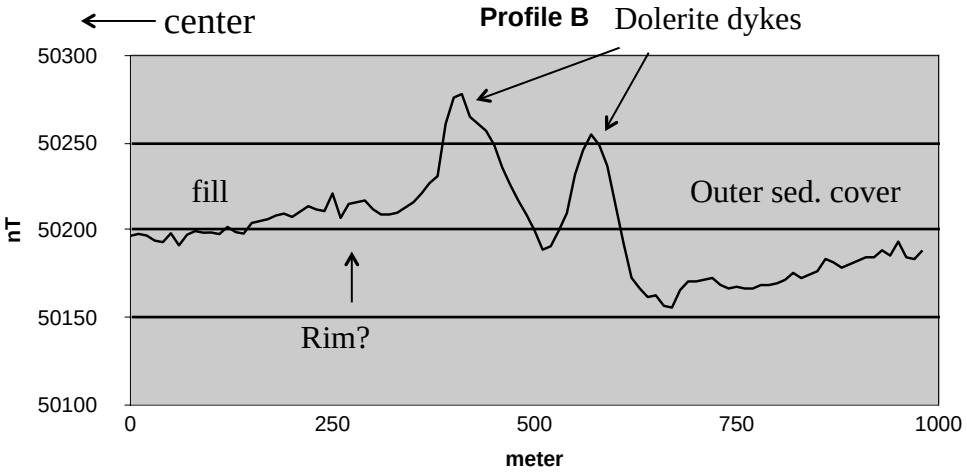

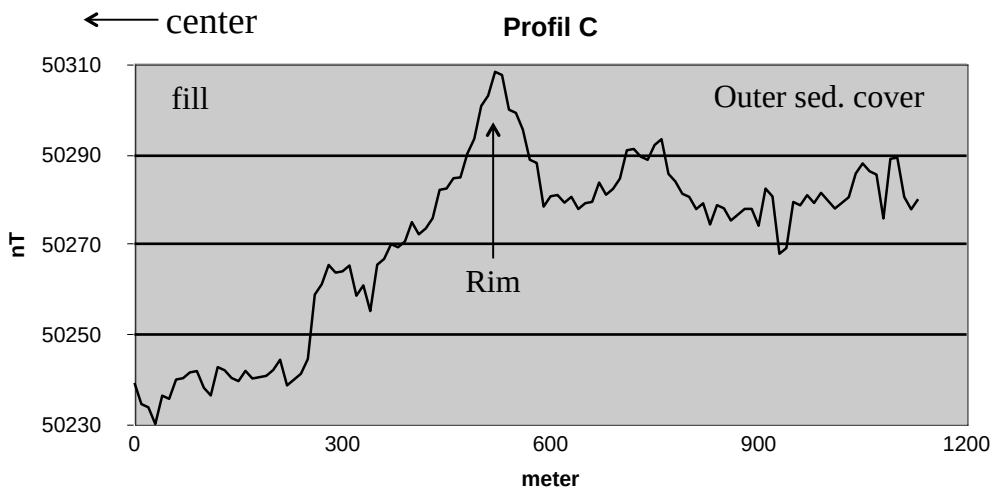

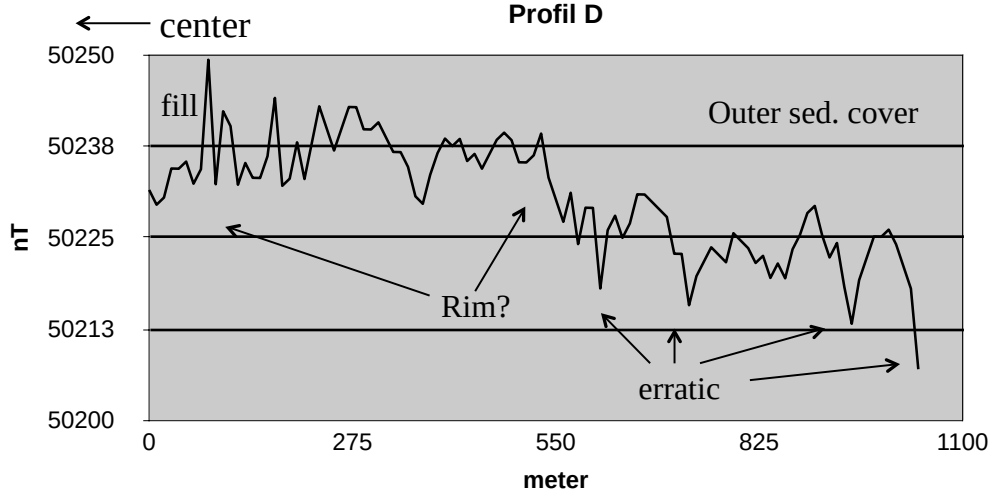

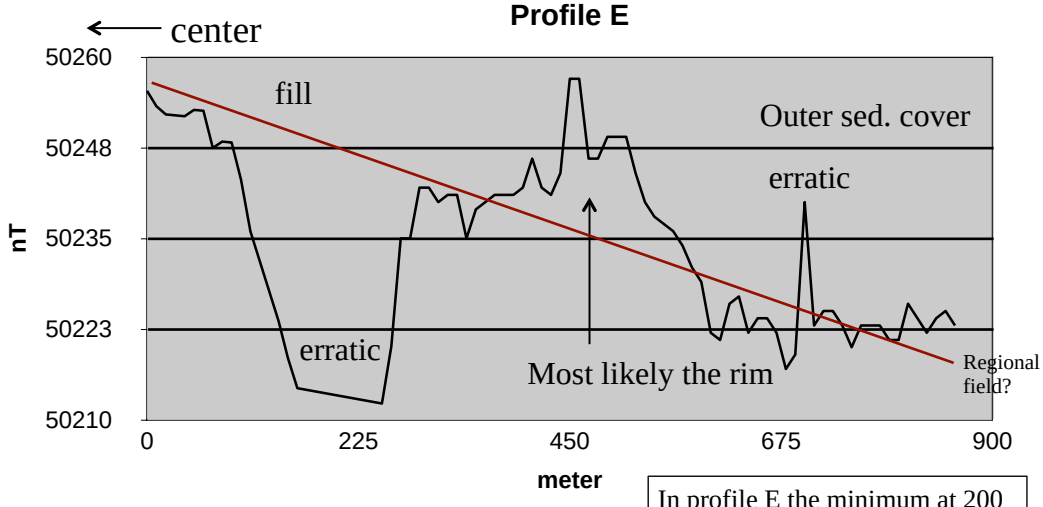

In profile E the minimum at 200 meters is deeper but the lowest values is removed
to enhance the scale of the profile.

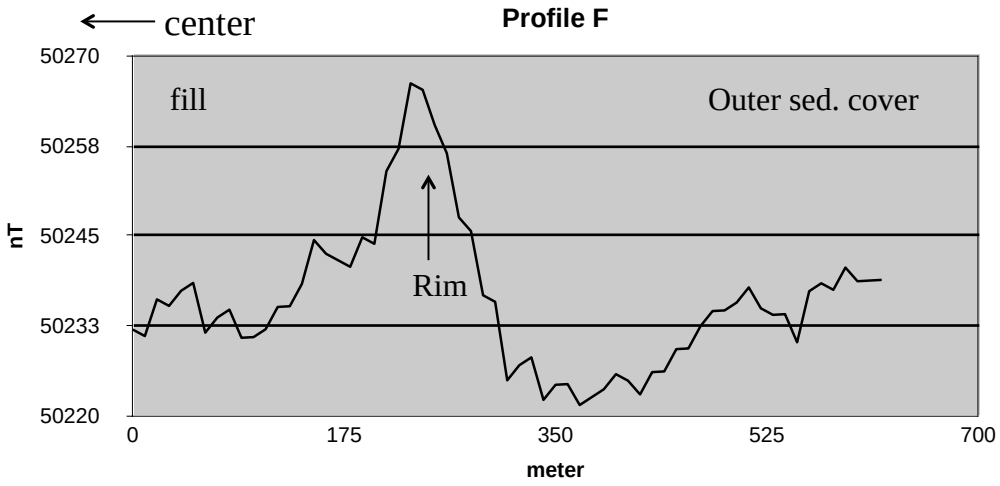

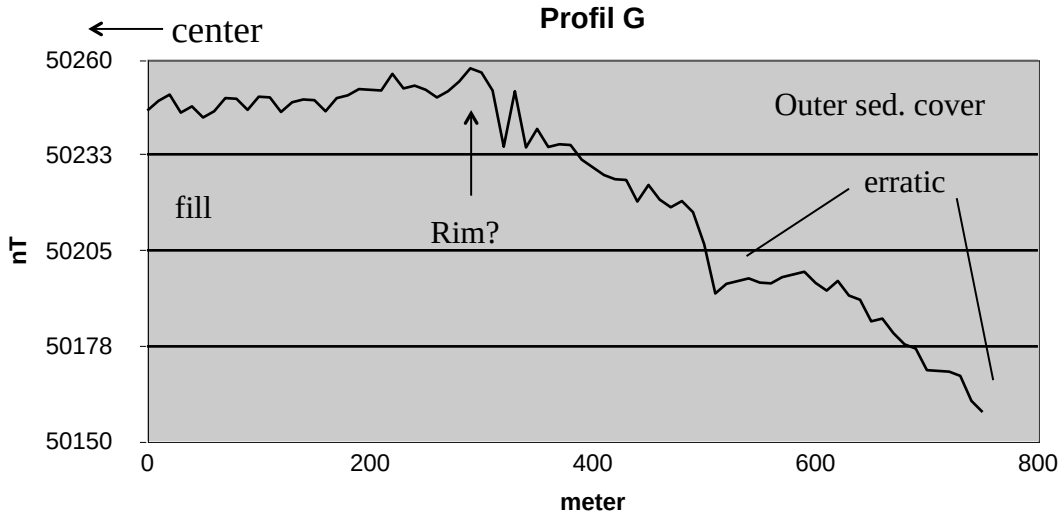

Co-ordinates
for the profiles:

A1 1450009 6479373	D1 1447727 6479205
A2 1450125 6479511	D2 1448694 6478731
A3 1450135 6479550	E1 1448514 6478705
A4 1450325 6479902	E2 1448263 6478609
B1 1449777 6479094	E3 1447704 6478413
B2 1450016 6479240	F1 1448305 6478083
B3 1450690 6479671	F2 1447815 6477697
C1 1449128 6480590	G1 1447340 6478068
C2 1449097 6480330	G2 1447736 6478280

Appendix 5 – Magnetic models from GMM (C & F)

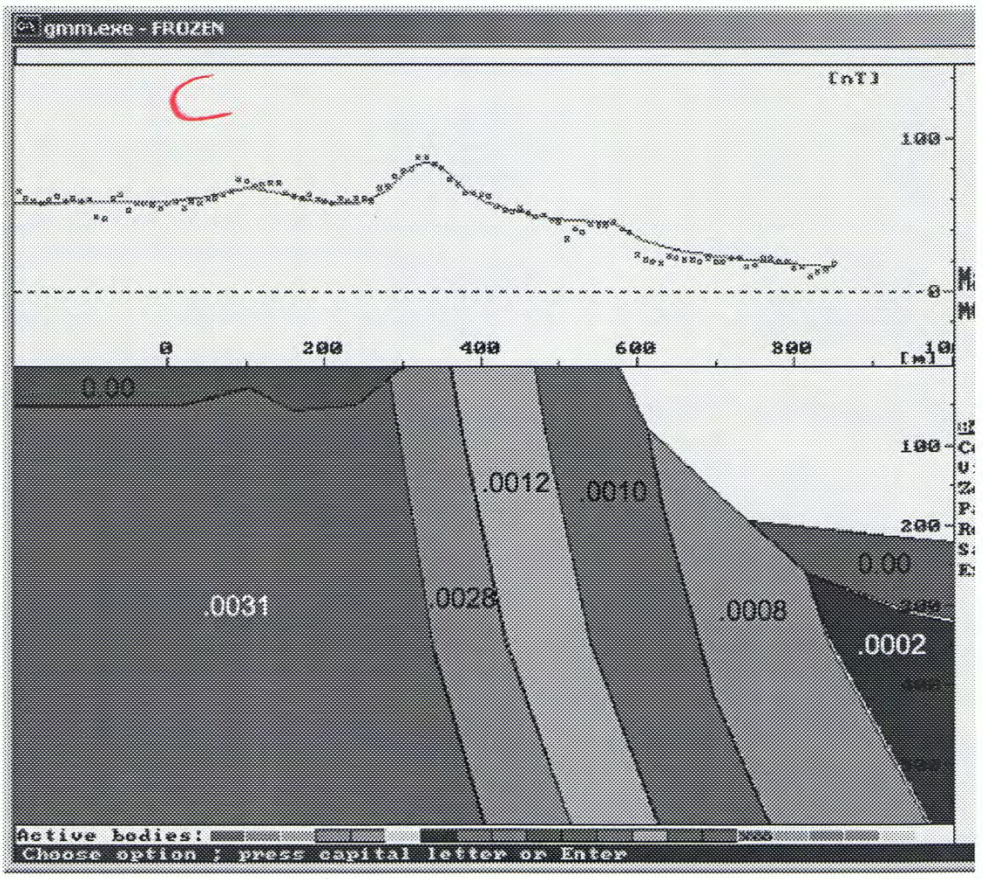

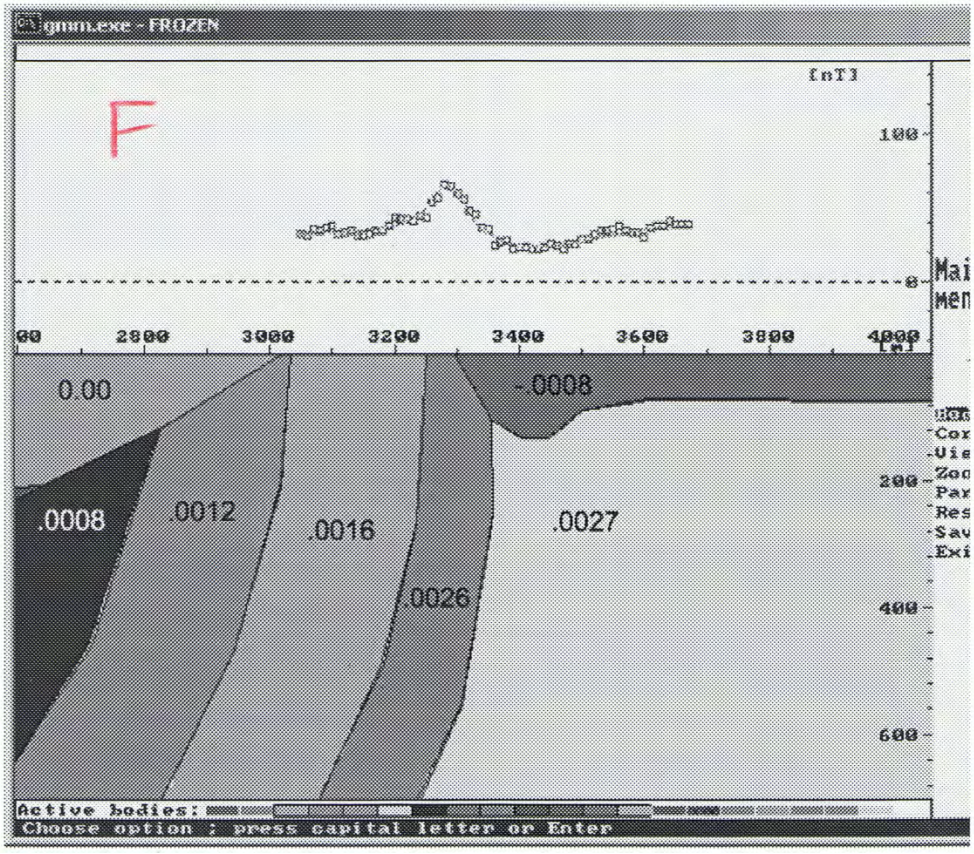

Appendix 6 – Susceptibility readings

Susceptibilities were measured on those cores reaching down into the basement. Since no susceptibility was found in the sediments only the numbers for the basement were registered.

Core	BH 2		BH 3		BH 5	
	depth (m)	*Susc. (*10^{-5} SI)*	*depth (m)*	*Susc. (*10^{-5} SI)*	*depth (m)*	*Susc. (*10^{-5} SI)*
	198,2	10	349	5	10,16	80
	198,95	10	350,85	20	10,3	55
	199,7	5	351,5	20	10,38	60
	200,7	5	353,6	25	10,45	70
	201,75	15	353,7	7	10,61	20
	203	15			10,98	5
	204,5	5			14,8	5
	205	5				
	206,5	10				

Core	BH 7		BH 8	
	depth (m)	*Susc. (*10^{-5} SI)*	*depth (m)*	*Susc. (*10^{-5} SI)*
	10,05	25	221,3	5
	10,25	20		
	10,35	10		
	10,4	0		
	10,5	5		
	10,65	10		
	10,75	25		
	10,85	20		

Appendix 7

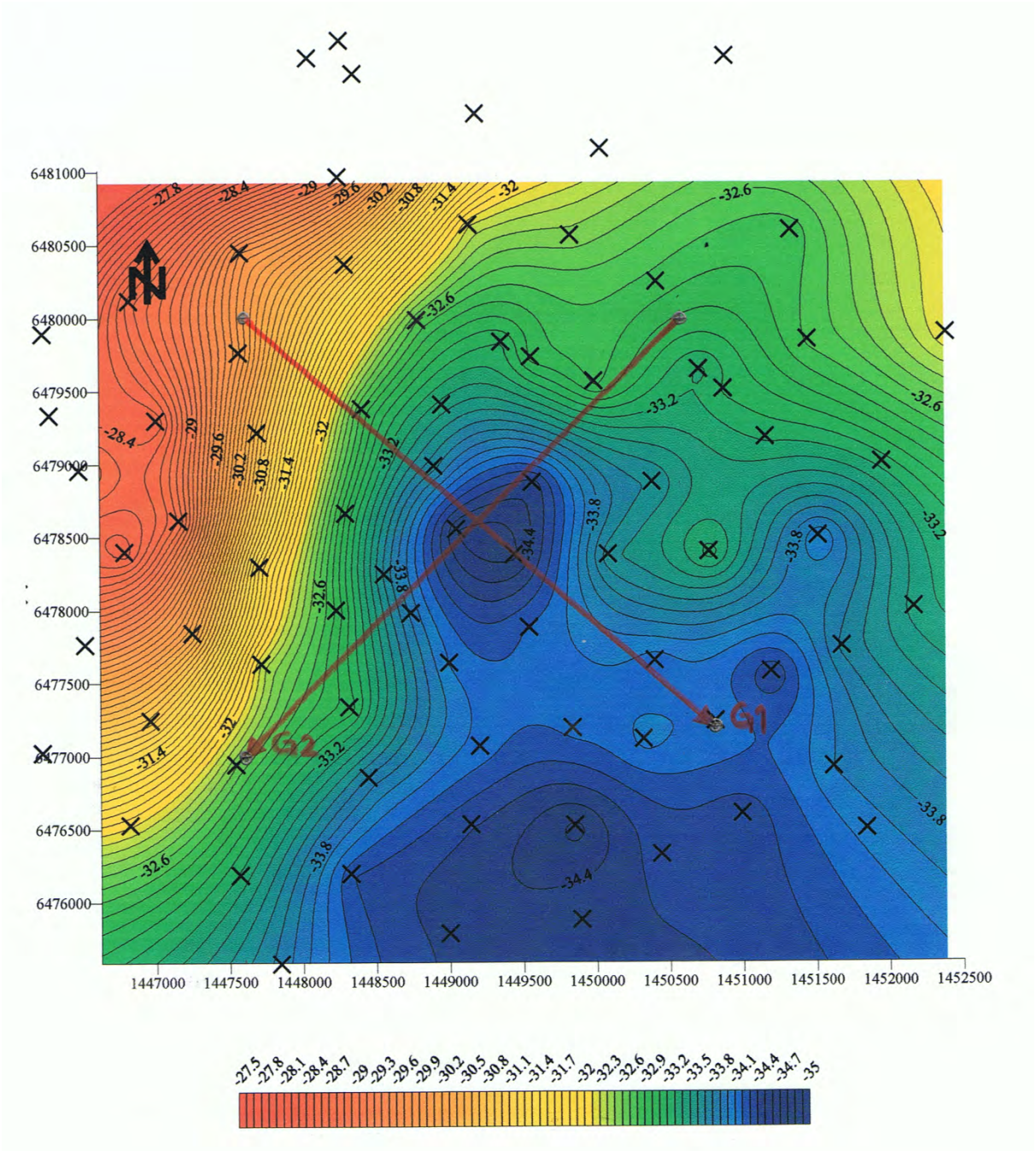

The picture shows the uncorrected gravity map with measurement points (not all) and gravity profiles G1 and G2.